

# Active Learning of Piecewise Gaussian Process Surrogates

Chiwoo Park<sup>1</sup>, Robert Waelder<sup>2</sup>, Bonggwon Kang<sup>3</sup>, Benji Maruyama<sup>2</sup>,  
Soondo Hong<sup>3</sup>, Robert Gramacy<sup>4</sup>

July 25, 2024

## Abstract

Active learning of Gaussian process (GP) surrogates has been useful for optimizing experimental designs for physical/computer simulation experiments, and for steering data acquisition schemes in machine learning. In this paper, we develop a method for active learning of piecewise, Jump GP surrogates. Jump GPs are continuous within, but discontinuous across, regions of a design space, as required for applications spanning autonomous materials design, configuration of smart factory systems, and many others. Although our active learning heuristics are appropriated from strategies originally designed for ordinary GPs, we demonstrate that additionally accounting for model bias, as opposed to the usual model uncertainty, is essential in the Jump GP context. Toward that end, we develop an estimator for bias and variance of Jump GP models. Illustrations, and evidence of the advantage of our proposed methods, are provided on a suite of synthetic benchmarks, and real-simulation experiments of varying complexity.

*Keywords:* Piecewise Regression, Divide-and-Conquer, Bias–Variance Tradeoff, Sequential Design, Active Learning

---

Author affiliation - 1: Department of Industrial and Systems Engineering, University of Washington, 2: Materials and Manufacturing Directorate, Air Force Research Lab, 3: Department of Industrial Engineering, Pusan National University, 4: Department of Statistics, Virginia Tech. The main algorithm of this work is protected by a provisional patent pending with application number 63/386,823.

# 1 Introduction

The main goal of machine learning is to create an autonomous computer system that can learn from data with minimal human intervention (Mitchell 1997). In many machine learning tasks, one can control the data acquisition process in order to select training examples that target specific goals. Active learning (AL) – or sequential design of experiments in classical statistical jargon – is the study of how to select data toward optimizing a given learning objective (e.g., Cohn et al. 1996, Lam & Notz 2008). Here we consider AL for piecewise continuous Gaussian process (GP) regression models.

Our motivating application is surrogate modeling (Gramacy 2020) of modern engineering systems, to explore and understand overall system performance and ultimately to optimize aspects of their design. A particular focus here is on engineering systems whose behaviors intermittently exhibit abrupt jumps or local discontinuities across regimes of a design space. Such “jump system” behaviors are found in many applications. For example, carbon nanotube yield from a chemical vapor deposition (CVD) process (Magrez et al. 2010) varies depending on many design variables. Changes in dynamics are mostly gradual, but process yield can suddenly jump around, depending on chemical equilibrium conditions, from ‘no-growth’ to ‘growth’ regions (Nikolaev et al. 2016). Specific boundary conditions dictating these regime shifts depend on experimental and system design details. Such jump system behaviors are universal to many material and chemistry applications owing to several factors (i.e., equilibrium, phase changes, activation energy). Jump behaviors are also frequently seen in engineering systems operating near capacity. When a system runs below its capacity, performance is generally good and exhibits little fluctuation. However, performance can suddenly break down as the system is forced to run slightly over its capacity (Kang et al. 2022).

Suitable surrogate models for jump systems must accommodate piecewise continuous functional relationships, where disparate input–output dynamics can be learned (if data from the process exemplify them) in geographically distinct regions on input/configuration space. Most existing surrogate modeling schemes make an assumption of stationarity, and are thus not well-suited to such processes. AL strategies paired with such surrogates are, consequently, sub-optimal for acquiring training examples in such settings. For example,

Gaussian processes (GPs; Rasmussen & Williams 2006) are perhaps the canonical choice for surrogate modeling of physical and computer experiments (Santner et al. 2018). They are flexible, nonparametric, nonlinear, lend a degree of analytic tractability, and provide well-calibrated uncertainty quantification without having to tune many unknown quantities. But the canonical, relative-distance-based kernels used with GPs result in stationary processes. Therefore, AL schemes paired with GPs exhibit un-interesting, space-filling behavior. Representative examples includes “Active Learning Cohn” (Cohn et al. 1996, ALC), “Active Learning-MacKay” (McKay et al. 2000, ALM), and “Active Learning with Mutual Information” (Krause et al. 2008, Beck & Guillas 2016, MI). Space-filling designs, and their sequential analogues, are inefficient when input–output dynamics change across regions of the input space. Intuitively, we need a higher density of training examples in harder-to-model regions, and near boundaries where regime dynamics change.

Regime-changing dynamics are inherently non-stationary: both position and relative distance information (in the input configuration space) is required for effective modeling. Examples of non-stationary GP modeling strategies from the geospatial literature abound (Sampson & Guttorp 1992, Schmidt & O’Hagan 2003, Paciorek & Schervish 2006). The trouble with these approaches is that they are too slow, in many cases demanding enormous computational resources in their own right, or limited to two input dimensions. Recent developments in the machine learning literature around deep GPs (Damianou & Lawrence 2013) represent a promising alternative. Input dimensions can be larger, and fast inference is provided by doubly stochastic variational inference (Salimbeni & Deisenroth 2017). But such methods are data-hungry, requiring tens of thousands of training examples before they are competitive with conventional GP methods. An ALC-type active learning criterion has been developed for deep GPs (Sauer et al. 2020), making them less data-hungry but computational expense for Markov chain Monte Carlo (MCMC) inference is still a bottleneck.

A class of methods built around divide-and-conquer strategies can offer the best of both worlds – computational thrift with modeling fidelity – by simultaneously imposing statistical and computational independence. The best-known examples include treed GPs (Gramacy & Lee 2008, Taddy et al. 2011, Malloy & Nowak 2014, Konomi et al. 2014)

and Voronoi tessellation-based GPs (Kim et al. 2005, Heaton et al. 2017, Pope et al. 2021, Luo et al. 2021). Partitioning facilitates non-stationarity almost trivially, by independently fitting different GPs in different parts of the input space. But learning the partition can be challenging. Sequential design/AL criteria have been adapted to some of these divide-and-conquer surrogates. ALM and ALC, for example, have been adapted for treed GPs (Gramacy & Lee 2009, Taddy et al. 2011). However the axis-aligned nature of the treed GP is not flexible enough to handle the complex, nonlinear manifold of regime change exhibited of many real datasets.

Park (2022) introduced the Jump GP to address this limitation. This approach seeks a local approximation to an otherwise potentially complex domain-partitioning and GP-modeling scheme. Crucially, direct inference for the Jump GP enjoys the same degree of analytic tractability as an ordinary, stationary GP. However, good AL strategies have not been studied for the Jump GP model, which is the main focus of this paper. We are inspired by related work in jump kernel regression (Park et al. 2023). However, it is important to remark that that work focused on a more limited class of (non-GP) nonparametric regression models. In the context of the Jump GP for nonstationary surrogate modeling, we propose to extend conventional AL strategies to consider model bias in addition to the canonical variance-based heuristics. We show that considering bias is essential in a non-stationary modeling setting. In particular, ordinary stationary GP surrogates may show significant biases at test locations near regime changes. The Jump GP can help mitigate this bias, but it does not completely remove it. The AL strategies that don't incorporate estimates of bias are limited in their ability to improve sequential learning of the Jump GP. The major contribution of this paper is to estimate both bias and variance for Jump GPs and parlay these into novel AL strategies for nonstationary surrogate modeling.

The remainder of the paper is outlined as follows. In Section 2, we review relevant topics around the Jump GP and AL with an eye toward motivating our novel contribution. Section 3 develops joint bias and variance estimation for Jump GPs. Using those estimates, we develop four AL heuristics for Jump GPs in Section 4. We illustrate the numerical performance of the proposed heuristics using four synthetic benchmarks and two real data/simulation cases in Section 5. A summary and brief discussion conclude the paper

in Section 6.

## 2 Review

Here we review components essential to framing our contribution: GP surrogates, AL, partition-based modeling and the Jump GP.

### 2.1 Stationary GP surrogates

Let  $\mathcal{X}$  denote a  $d$ -dimensional input configuration space. Consider a problem of estimating an unknown function  $f : \mathcal{X} \rightarrow \mathbb{R}$  relating inputs  $\mathbf{x}_i \in \mathcal{X}$  to a noisy real-valued response variable  $y_i \stackrel{\text{iid}}{\sim} \mathcal{N}(f(\mathbf{x}_i), \sigma^2)$  though examples composed as training data,  $\mathcal{D}_N = \{(\mathbf{x}_i, y_i), i = 1, \dots, N\}$ . In GP regression, a finite collection  $\mathbf{f}_N = (f_1, \dots, f_N)$  of  $f(\mathbf{x}_i) \equiv f_i$  values is modeled as a multivariate normal (MVN) random variable. A common specification involves a constant, scalar mean  $\mu$ , and  $N \times N$  correlation matrix  $\mathbf{C}_N$ :  $\mathbf{f}_N \sim \mathcal{N}_N(\mu \mathbf{1}_N, \mathbf{C}_N)$ .

Rather than treating all  $\mathcal{O}(N^2)$  values in  $\mathbf{C}_N$  as “tunable parameters”, it is common to use a kernel  $c(\mathbf{x}_i, \mathbf{x}_j; \theta)$  defining correlations in terms of a small number of hyperparameters  $\theta$ . Most kernel families (Abrahamsen 1997, Wendland 2004) are decreasing functions of the geographic “distance” between its arguments  $\mathbf{x}_i$  and  $\mathbf{x}_j$ . Our contributions are largely agnostic to these choices. An assumption of *stationarity* is common, whereby  $c(\mathbf{x}_i, \mathbf{x}_j; \theta) \equiv c(\mathbf{x}_i - \mathbf{x}_j; \theta)$ , i.e., only relative displacement  $\mathbf{x}_i - \mathbf{x}_j$  between inputs, not their positions, matters for modeling. As discussed further, below, a stationarity assumption can be limiting and relaxing this is a major focus of the methodology introduced in this paper.

Integrating out latent  $\mathbf{f}_N$  values, to obtain a distribution for  $\mathbf{y}_N$ , is straightforward because both are Gaussian. This leads to the marginal likelihood  $\mathbf{y}_N \sim \mathcal{N}_N(\mu \mathbf{1}_N, \mathbf{C}_N + \sigma^2 \mathbb{I}_N)$  which can be used to learn hyperparameters. Maximum likelihood estimates (MLEs),  $\hat{\mu}$  and  $\hat{\sigma}^2$ , have closed forms conditional on  $\theta$ . E.g., Mu et al. (2017) provides  $\hat{\mu} = \mathbf{1}_N^T (\hat{\sigma}^2 \mathbf{I}_N + \mathbf{C}_N)^{-1} \mathbf{y}_N / \mathbf{1}_N^T (\hat{\sigma}^2 \mathbf{I}_N + \mathbf{C}_N)^{-1} \mathbf{1}_N$ . Estimates for  $\hat{\theta}$  depend on the kernel and generally requires numerical methods. For details, see Rasmussen & Williams (2006), Santner et al. (2018), Gramacy (2020).

Analytic tractability extends to prediction. Basic MVN conditioning from a joint model

of  $\mathbf{Y}_N$  and an unknown testing output  $Y(\mathbf{x}_*)$  gives that  $Y(\mathbf{x}_*) \mid \mathbf{y}_N$  is univariate Gaussian. Below we quote the distribution for the latent function value  $\hat{f}(\mathbf{x}) \equiv f(\mathbf{x}_*) \mid \mathbf{y}_N$ , which is of more direct interest in our setting. This distribution is also Gaussian, with

$$\begin{aligned} \text{mean:} \quad & \mu(\mathbf{x}_*) = \hat{\mu} + \mathbf{c}_N^T (\sigma^2 \mathbf{I}_N + \mathbf{C}_N)^{-1} (\mathbf{y}_N - \hat{\mu} \mathbf{1}_N), \text{ and} \\ \text{variance:} \quad & s^2(\mathbf{x}_*) = c(\mathbf{x}_*, \mathbf{x}_*; \hat{\theta}) - \mathbf{c}_N^T (\hat{\sigma}^2 \mathbb{I}_N + \mathbf{C}_N)^{-1} \mathbf{c}_N, \end{aligned} \tag{1}$$

where  $\mathbf{c}_N = [c(\mathbf{x}_i, \mathbf{x}_*; \hat{\theta}) : i = 1, \dots, N]$  is a  $N \times 1$  vector of the covariance values between the training data and the test data point. Observe that evaluating these prediction equations, like evaluating the MVN likelihood for hyperparameter inference, requires inverting the  $N \times N$  matrix  $\mathbf{C}_N$ . So although there is a high degree of analytic tractability, there are still substantial numerical hurdles to application in large-data settings.

## 2.2 Divide-and-conquer GP modeling

Partitioned GP models (Gramacy & Lee 2008, Kim et al. 2005), generally, and the Jump GP (Park 2022), specifically, consider an  $f$  that is piecewise continuous

$$f(\mathbf{x}) = \sum_{k=1}^K f_k(\mathbf{x}) 1_{\mathcal{X}_k}(\mathbf{x}), \tag{2}$$

where  $\mathcal{X}_1, \mathcal{X}_2, \dots, \mathcal{X}_K$  are a partition of  $\mathcal{X}$ . Above,  $1_{\mathcal{X}_k}(\mathbf{x})$  is an indicator function that determines whether  $\mathbf{x}$  belongs to region  $\mathcal{X}_k$ , and each  $f_k(\mathbf{x})$  is a continuous function that serves as a basis for the regression model on region  $\mathcal{X}_k$ . Although variations abound, here we take each functional piece  $f_k(\mathbf{x})$  to be a stationary GP, as described in Section 2.1.

Typically, each  $f_k$  is taken to independent conditional on the partitioning mechanism. This assumption is summarized below for easy referencing later.

$$\text{Independence:} \quad f_k \text{ is independent of } f_j \text{ for } j \neq k. \tag{3}$$

Consequently, all hyperparameters describing  $f_k$  may be analogously indexed and are treated independently, e.g.,  $\mu_k$ ,  $\sigma_k^2$  and  $\theta_k$ . Generally speaking, the data within region  $\mathcal{X}_k$  are used to learn these hyperparameters, via the likelihood applied on the subset of data  $\mathcal{D}_N$  whose  $\mathbf{x}$ -locations reside in  $\mathcal{X}_k$ . Although it is possible to allow novel kernels  $c_k$  in each region, it is common to fix a particular form (i.e., a family) for use throughout. Only

it’s hyperparameters  $\theta_k$  vary across regions, as in  $c(\cdot, \cdot; \theta_k)$ . Predicting with  $\hat{f}(\mathbf{x}_*)$ , conditional on a partition and estimated hyperparameters, is simply a matter of following Eq. (2) with “hats”. That is, with  $\hat{f}_k$  defined analogously to Eq. (1), i.e., using only  $y$ -values exclusive to each region. In practice, the sum over indicators in Eq. (2) is bypassed and one simply identifies the  $\mathcal{X}_k$  to which  $\mathbf{x}_*$  belongs and uses the corresponding  $\hat{f}_k$  directly.

Popular, data-driven partitioning schemes leveraging local stationary GP models include Voronoi tessellation (Kim et al. 2005, Heaton et al. 2017, Pope et al. 2021, Luo et al. 2021) or recursive axis-aligned, tree-based partitioning (Gramacy & Lee 2008, Taddy et al. 2011, Malloy & Nowak 2014, Konomi et al. 2014). These “structures”, defining  $K$ , and within-partition hyperparameters  $(\mu_k, \theta_k, \sigma^2)$  may be jointly learned, via posterior sampling (e.g., MCMC) or by maximizing marginal likelihoods. In so doing, one is organically learning a degree of non-stationarity. Independent GPs, via disparate independently learned hyperparameters, facilitate a position-dependent correlation structure. Learning separate  $\sigma_k^2$  in each region can also accommodate heteroskedasticity (Binois et al. 2018). Such divide-and-conquer can additionally bring computational gains, through smaller- $N$  calculations within each region of the partition.

### 2.3 Local GP modeling

Although there are many example settings where such partition-based GP models excel, their rigid structure can be a mismatch to many important real-data settings. The Jump GP (JGP; Park 2022) is motivated by such applications. The idea is best introduced through the lens of local, approximate GP modeling (LAGP; Gramacy & Apley 2015). For each test location  $\mathbf{x}_*$ , select a small subset of training data nearby  $\mathbf{x}_*$ :  $\mathcal{D}_n(\mathbf{x}_*) = \{(\mathbf{x}_{i,*}, y_{i,*})\}_{i=1}^n \subset \mathcal{D}_N$ . Then, fit a conventional, stationary GP model  $\hat{f}_n(\mathbf{x}_*)$  to the local data  $\mathcal{D}_n(\mathbf{x}_*)$ . This is fast, because  $\mathcal{O}(n^3)$  is much better than  $\mathcal{O}(N^3)$  when  $n \ll N$ , and massively parallelizable over many  $\mathbf{x}_* \in \mathcal{X}$  (Gramacy et al. 2014). It has a nice divide-and-conquer structure, but it is not a partition model (2). Nearby  $\mathcal{D}_n(\mathbf{x}'_*)$  might have some, all, or no elements in common. LAGP can furnish biased predictions (Park 2022) because independence (3) is violated: local data  $\mathcal{D}_n(\mathbf{x}'_*)$  might mix training examples from regions of the input space exhibiting disparate input-output dynamics.

A JGP differs from basic LAGP modeling by selecting local data subsets in such a way as a partition (2) is maintained and independence (3) is enforced, so that bias is reduced. Toward this end, the JGP introduces an latent, binary random variable  $Z_i \in \{0, 1\}$  to express uncertainties on whether a local data point  $\mathbf{x}_{i,*}$  belongs to a region of the input exhibiting the same (stationary) input-output dynamics as the test location  $\mathbf{x}_*$ , or not:

$$Z_i = \begin{cases} 1 & \text{if } \mathbf{x}_{i,*} \text{ and } \mathbf{x}_* \text{ belong to the same region} \\ 0 & \text{otherwise.} \end{cases}$$

Conditional on  $Z_i$  values,  $i = 1, \dots, N$ , we may partition the local data  $\mathcal{D}_n$  into two groups:  $\mathcal{D}_* = \{i = 1, \dots, n : Z_i = 1\}$  and  $\mathcal{D}_o = \{1, \dots, n\} \setminus \mathcal{D}_*$ , lying in regions of the input space containing  $\mathbf{x}_*$  and not, respectively.

Complete the specification by modeling  $\mathcal{D}_*$  with a stationary GP [Section 2.1],  $\mathcal{D}_o$  with dummy likelihood  $p(y_{i,*} | Z_i = 0) \propto U$  for some constant,  $U$ , and assign a prior for the latent variable  $Z_i$  via a sigmoid  $\pi$  on an unknown partitioning function  $g(\mathbf{x}, \boldsymbol{\omega})$ ,

$$p(Z_i = 1 | \mathbf{x}_{i,*}, \boldsymbol{\omega}) = \pi(g(\mathbf{x}_{i,*}, \boldsymbol{\omega})), \quad (4)$$

where  $\boldsymbol{\omega}$  is another hyperparameter. The form of the parametric partitioning function  $g$  influences the boundary dividing  $\mathcal{D}_o$  and  $\mathcal{D}_*$ . At the local level, linear or quadratic  $g$  serves a good local Taylor approximation to complex domain boundaries. For a detailed discussion, one may refer to Park (2022). Here we take the linear form  $g(\mathbf{x}) = \boldsymbol{\omega}^T [1, \mathbf{x}]$ .

Specifically, for  $\mathbf{Z} = (Z_i, i = 1, \dots, n)$ ,  $\mathbf{f}_* = (f_{i,*}, i = 1, \dots, n)$  and  $\Theta = \{\boldsymbol{\omega}, m_*, \theta_*, \sigma^2\}$ , the JGP model may be summarized as follows.

$$\begin{aligned} p(\mathbf{y}_n | \mathbf{f}_*, \mathbf{Z}, \Theta) &= \prod_{i=1}^n \mathcal{N}_1(y_{i,*} | f_{i,*}, \sigma^2)^{Z_i} U^{1-Z_i}, \\ p(\mathbf{Z} | \boldsymbol{\omega}) &= \prod_{i=1}^n \pi(g(\mathbf{x}_{i,*}, \boldsymbol{\omega}))^{Z_i} (1 - \pi(g(\mathbf{x}_{i,*}, \boldsymbol{\omega})))^{1-Z_i}, \\ p(\mathbf{f}_* | m_*, \theta_*) &= \mathcal{N}_n(\mathbf{f}_* | m_* \mathbf{1}_n, \mathbf{C}_{nn}), \end{aligned}$$

where  $\mathbf{y}_n = (y_{i,*}, i = 1, \dots, n)$  and  $\mathbf{C}_{nn} = [c(\mathbf{x}_{i,*}, \mathbf{x}_{j,*}; \theta_*) : i, j = 1, \dots, n]$  is a square matrix of the covariance values evaluated for all pairs of the local data  $\mathcal{D}_n(\mathbf{x}_*)$ .

Conditional on  $\Theta$ , prediction  $\hat{f}(\mathbf{x}_*)$  follows the usual equations (1) using local data  $\mathcal{D}_n(\mathbf{x}_*)$ . A detailed presentation is delayed, along with further discussion, until Section



3. Inference for latent  $\mathbf{Z}$  may proceed by expectation maximization (EM; Dempster et al. 1977). However, a difficulty arises because the joint posterior distribution of  $\mathbf{Z}$  and  $\mathbf{f}_*$  is not tractable, complicating the E-step. As a workaround, Park (2022) developed a *classification EM* (CEM; Bryant & Williamson 1978, Gupta & Chen 2010) variation which replaces the E-step with a pointwise maximum *a posteriori* (MAP) of  $\hat{\mathbf{Z}}$ .

## 2.4 Active Learning for GPs

Active learning (AL) attempts to sustain a virtuous cycle between data collection and model learning. Begin with training data of size  $N$ ,  $\mathcal{D}_N = \{(\mathbf{x}_i, y_i), i = 1, \dots, N\}$ , such as a space-filling Latin hypercube design (LHD; Lin & Tang 2015). Then augment  $\mathcal{D}_N$  with a new data point  $(\mathbf{x}_{N+1}, y_{N+1})$  chosen to optimize a criterion quantifying an important aspect or capability of the model, and repeat. Perhaps the canonical choice is mean square prediction error (MSPE), comprising of squared bias and variance (Hastie et al. 2009).

Many machine learning algorithms are equipped with proofs of unbiasedness of predictions under regularity conditions. When training and testing data jointly satisfy a stationarity assumption, the GP predictor (1) is unbiased, and so the MSPE is equal to  $s^2(\mathbf{x}_*)$ . Consequently, many AL leverage this quantity. For example, “Active Learning-MacKay” (ALM; McKay et al. 2000) maximizes it directly:  $\mathbf{x}_{N+1} = \operatorname{argmax}_{\mathbf{x}_* \in \mathcal{X}} s(\mathbf{x}_*)$ . In repeated application, this AL strategy can be shown to approximate a maximum entropy design (Gramacy 2020, Section 6.3).

An integrated mean squared prediction error (IMSPE) criterion considers how the MSPE of GP is affected, globally in the input space, *after* injecting new data at  $\mathbf{x}_{N+1}$ . Let  $s_{N+1}^2(\mathbf{x}_*)$  denote the predictive variance (1) a test location  $\mathbf{x}_*$ , when the training data  $\mathcal{D}_N$  is augmented with one additional input location  $\mathbf{x}_{N+1}$ :

$$s^2(\mathbf{x}_*; \mathbf{x}_{N+1}) = c(\mathbf{x}_*, \mathbf{x}_*; \hat{\theta}) - \mathbf{c}_{N+1}^T (\hat{\sigma}^2 \mathbf{I}_{N+1} + \mathbf{C}_{N+1})^{-1} \mathbf{c}_{N+1},$$

where  $\mathbf{c}_{N+1} = [c(\mathbf{x}_i, \mathbf{x}_*; \hat{\theta}) : i = 1, \dots, N + 1]$ ,  $\mathbf{C}_{N+1}$  analogously via  $\hat{\theta}$  via  $\mathcal{D}_N$ . Then,

$$\text{IMSPE}(\mathbf{x}_{N+1}) = \int_{\mathcal{X}} s(\mathbf{x}_*; \mathbf{x}_{N+1}) d\mathbf{x}_*,$$

which has a closed form (Binois et al. 2019), although in machine learning an quadrature-based version called “Active Learning Cohn” (Cohn et al. 1996, ALC) is preferred.

Such variance-only criteria make sense when data satisfies the unbiasedness condition, i.e., under stationarity, which can be egregiously violated in many real-world settings. In Bayesian optimization contexts, acquisition criteria have been extended to account for this bias (Lam & Notz 2008, Mu et al. 2017), but we are not aware of any analogous work for AL targeting overall accuracy. A major focus of this paper is to develop bias and variance estimates for JGP and leverage them to improve the active learning of JGP.

### 3 Bias–variance decomposition for JGPs

The following discussion centers around predictive equations for a JGP: essentially Eq. (1) with  $\mathcal{D}_n(\mathbf{x}_*)$ . For convenience, these are re-written here, explicitly in that JGP notation. Let  $\hat{Z}_i$  represent the MAP estimate at convergence (of the CEM algorithm) and let  $\mathcal{D}_{n,*} = \{i = 1, \dots, n : \hat{Z}_i = 1\}$  denote the estimate of  $\mathcal{D}_*$  with  $n_*$  being the number of training data pairs in the set. Conditional on  $\hat{\Theta}$ , the posterior predictive distribution of  $\hat{f}_*(\mathbf{x})$  at a test location  $\mathbf{x}_*$  is univariate Gaussian with

$$\begin{aligned} \text{mean:} \quad & \mu_J(\mathbf{x}_*) = \hat{m}_* + \mathbf{c}_*^T (\hat{\sigma}^2 \mathbf{I}_{n_*} + \mathbf{C}_{**})^{-1} (\mathbf{y}_* - \hat{m}_* \mathbf{1}_{n_*}), \text{ and} \\ \text{variance:} \quad & s_J^2(\mathbf{x}_*) = c(\mathbf{x}_*, \mathbf{x}_*; \hat{\theta}_*) - \mathbf{c}_*^T (\hat{\sigma}^2 \mathbf{I}_{n_*} + \mathbf{C}_{**})^{-1} \mathbf{c}_*, \end{aligned} \tag{5}$$

where  $\mathbf{y}_* = [y_i : i \in \mathcal{D}_{n,*}]$  is a  $n_* \times 1$  vector of the selected local data,  $\mathbf{c}_* = [c(\mathbf{x}_{i,*}, \mathbf{x}_*; \theta_*) : i \in \mathcal{D}_{n,*}]$  is a column vector of the covariance values between  $\mathbf{y}_*$  and  $f(\mathbf{x}_*)$ , and  $\mathbf{C}_{**} = [c(\mathbf{x}_i, \mathbf{x}_j; \theta_*) : i, j \in \mathcal{D}_{n,*}]$  is a square matrix of the covariance values evaluated for all pairs of the selected local data. Here,  $\hat{\sigma}^2$  and  $\hat{\theta}_*$  represent the MLEs of  $\sigma^2$  and  $\theta_*$  respectively, and  $\hat{m}_*$  is the MLE of  $m_*$ , which has the form

$$\hat{m}_* = \frac{\mathbf{1}_{n_*}^T (\hat{\sigma}^2 \mathbf{I}_{n_*} + \mathbf{C}_{**})^{-1} \mathbf{y}_*}{\mathbf{1}_{n_*}^T (\hat{\sigma}^2 \mathbf{I}_{n_*} + \mathbf{C}_{**})^{-1} \mathbf{1}_{n_*}}. \tag{6}$$

Subsections which follow break down the mean  $\mu_J(\mathbf{x}_*)$  and variance  $s_J^2(\mathbf{x}_*)$  quoted in Eq. (5), in terms of their contribution to bias and variance of a JGP predictor, respectively, with an eye toward AL application in Section 4 as an estimator of MSPE:

$$\text{MSPE}[\mu_J(\mathbf{x}_*)] = \text{Bias}^2[\mu_J(\mathbf{x}_*)] + \text{Var}[\mu_J(\mathbf{x}_*)]. \tag{7}$$

### 3.1 Bias

The following theorem gives the theoretical bias of  $\mu_J(\mathbf{x}_*)$  under an assumption. The assumption would hold for most test points except where more than two regions are separated by a border. The proof of the theorem is placed in Appendix A.

**Theorem 1.** *Assume that the local data group  $\mathcal{D}_o$  is from one homogeneous region, which corresponds to the case that the local data  $\mathcal{D}_n(\mathbf{x}_*)$  come out from two regions with each of  $\mathcal{D}_*$  and  $\mathcal{D}_o$  being from one homogeneous region. The bias of  $\mu_J(\mathbf{x}_*)$  is*

$$\begin{aligned} \text{Bias}[\mu_J(\mathbf{x}_*)] &= (m_* - m_o) \sum_{j \in \mathcal{D}_{n,*}} \alpha_j \{(1 - p_j)p_* - p_j(1 - p_*)\} \\ &\quad + (m_* - m_o) \sum_{i \in \mathcal{D}_{n,*}} \sum_{j \in \mathcal{D}_{n,*}} \alpha_j \beta_i \{p_j(1 - p_i) - (1 - p_j)p_i\}, \end{aligned} \quad (8)$$

where  $m_o = \mathbb{E}[f(\mathbf{x}_*)|Z_* = 1]$  with  $Z_*$  standing for the latent  $Z$ -variable associated with test point  $\mathbf{x}_*$ ,  $\alpha_i$  is the  $i$ th element of  $\boldsymbol{\alpha} = \mathbf{1}_{n_*}^T (\sigma^2 \mathbf{I}_{n_*} + \mathbf{C}_{**})^{-1} / (\mathbf{1}_{n_*}^T (\sigma^2 \mathbf{I}_{n_*} + \mathbf{C}_{**})^{-1} \mathbf{1}_{n_*})$ ,  $p_* = p(Z_* = 1)$  and  $p_i = P(Z_i = 1)$ .

Evaluation this bias expression is not possible due to many unknown quantities such as  $m_*$ ,  $m_o$ ,  $p_*$  and  $p_i$ . We develop a plug-in estimate in this section and then provide a numerical evaluation later in Section 3.3.

The quantity  $m_*$  may be estimated by a local mean estimate  $\hat{\mu}_*$ . Similarly, with a uniform likelihood for  $\mathcal{D}_*$ ,  $m_o$  may be estimated via sample mean,

$$\hat{m}_o = \frac{1}{n - n_*} \sum_{i \in \mathcal{D}_n(\mathbf{x}_*) \setminus \mathcal{D}_{n,*}} y_{i,*}.$$

Probabilities  $p_j$  and  $p_*$  may be estimated via Eq. (4) with  $\boldsymbol{\omega}$  estimated by the JGP. Let  $\hat{p}_j$  and  $\hat{p}_*$  denote those estimates. Inserting them into (8) yields the following plug-in estimate:

$$\begin{aligned} \widehat{\text{Bias}}[\mu_J(\mathbf{x}_*)] &= (\hat{m}_* - \hat{m}_o) \sum_{j \in \mathcal{D}_{n,*}} \alpha_j \{(1 - \hat{p}_j)\hat{p}_* - \hat{p}_j(1 - \hat{p}_*)\} \\ &\quad + (\hat{m}_* - \hat{m}_o) \sum_{i \in \mathcal{D}_{n,*}} \sum_{j \in \mathcal{D}_{n,*}} \alpha_j \beta_i \{\hat{p}_j(1 - \hat{p}_i) - (1 - \hat{p}_j)\hat{p}_i\}. \end{aligned} \quad (9)$$

It is worth remarking that  $\widehat{\text{Bias}}[\mu_J(\mathbf{x}_*)]$  in Eq. (9) is influenced by accuracy of  $\hat{\mathbf{Z}}$ , or in other words by the classification accuracy of local data furnished by the CEM algorithm.

The first term in  $\widehat{\text{Bias}}[\mu_J(\mathbf{x}_*)]$  requires the summation of more non-zero terms as the probability that  $Z_j \neq Z_*$  increases (for the selected data  $\mathbf{y}_*$ ), i.e., when the selected data have low probabilities of being from the region of a test location. Conversely, the second term in  $\widehat{\text{Bias}}[\mathbf{x}_*]$  would require summing more non-zero terms as the total probabilities of the selected data  $\mathbf{y}_*$  (being from heterogeneous regions) increases, i.e., when the selected data are highly likely from heterogeneous regions. Some visuals will be provided momentarily in Section 3.4 along with a comprehensive illustration. But first, we wish to complete the MSPE decomposition (7) with an estimate of predictive variance.

## 3.2 Variance

The variance of  $\mu_J(\mathbf{x}_*)$  also depends on  $\mathbf{Z}$ . Conditional on  $\mathbf{Z}$ , this quantity is given by  $s_J^2(\mathbf{x}_*)$  in Eq. (5). To make this dependency explicit, we rewrite this variance as  $s_J^2(\mathbf{x}_*; \mathbf{Z})$ . The law of total probability can be used to obtain the overall variance of  $\mu_J(\mathbf{x}_*)$ , unconditional on  $\mathbf{Z}$ :

$$\text{Var}[\mu_J(\mathbf{x}_*)] = \sum_{\mathbf{Z} \in \mathbb{B}^n} s_J^2(\mathbf{x}_*; \mathbf{Z}) p(\mathbf{Z}), \quad (10)$$

where  $\mathbb{B}^n$  represents a collection of all possible  $n$ -dimensional binary values. Evaluating this expression (10) in practice is technically doable but cumbersome as the number of distinct settings of  $\mathbf{Z}$  grows as  $2^N$ . To streamline the evaluation, we prefer to short-circuit an exhaustive enumeration by bypassing *a posteriori* improbable settings, instead considering only  $\mathbf{Z}$ 's with high  $p(\mathbf{Z})$  values. Toward that, let  $\mathcal{B}_r(\hat{\mathbf{Z}}) = \{\mathbf{Z} \in \mathbb{B}^n : Z_j = \hat{Z}_j \text{ except for } r \text{ elements}\}$ . Since  $\mathbb{B}^n = \bigcup_{r=0}^n \mathcal{B}_r(\hat{\mathbf{Z}})$ , and  $\sum_{r=0}^n \sum_{\mathbf{Z} \in \mathcal{B}_r(\hat{\mathbf{Z}})} p(\mathbf{Z}) = 1$ , we have

$$\text{Var}[\mu_J(\mathbf{x}_*)] = \frac{\sum_{r=0}^n \sum_{\mathbf{Z} \in \mathcal{B}_r(\hat{\mathbf{Z}})} s_J^2(\mathbf{x}_*; \mathbf{Z}) p(\mathbf{Z})}{\sum_{r=0}^n \sum_{\mathbf{Z} \in \mathcal{B}_r(\hat{\mathbf{Z}})} p(\mathbf{Z})}, \quad (11)$$

where  $p(\mathbf{Z})$  can be estimated as  $\hat{p}(\mathbf{Z}) = \prod_{i=1}^n \hat{p}_i^{Z_i} (1 - \hat{p}_i)^{1-Z_i}$ .

Due to the nature of CEM inference, estimated  $\hat{p}_i$  are highly concentrated around 0 and 1. For example, consider a test function illustrated in Figure 1 (a). In the figure, we utilize a two-dimensional grid where the output value  $y(\mathbf{X})$  is indicated in grayscale. The test function is described in more detail momentarily in Section 3.4. Overlaid are 84 test locations as red dots. These are placed along a ridge in the response surface for

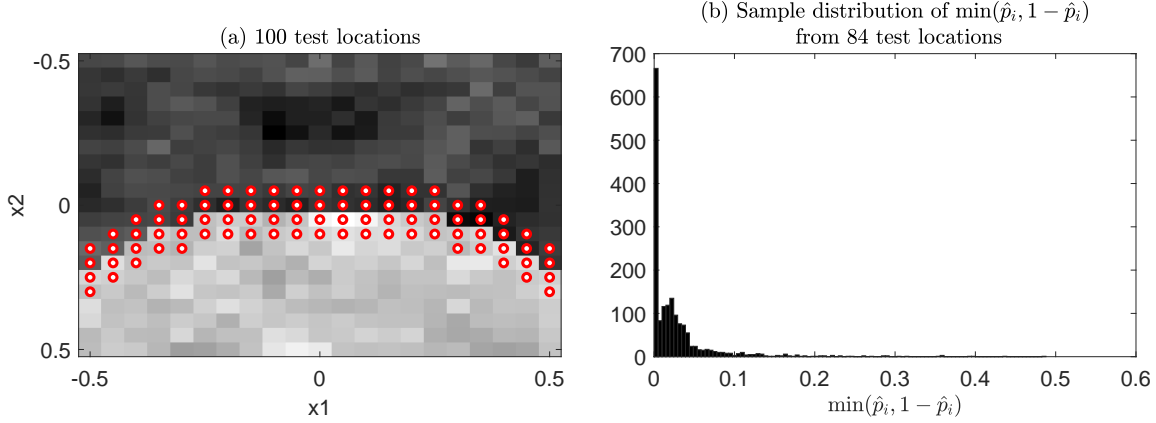


Figure 1: Empirical distribution of  $\hat{p}_i$  for a test function over a two-dimensional grid of  $(x_1, x_2)$  illustrated in (a).

dramatic effect. We set  $n = 20$ , which means that for each test location, JGP would condition on twenty local training data examples, and consequently CEM would provide  $\hat{p}_1, \dots, \hat{p}_n, n = 20$ , one for each. Figure 1 (b) shows how the  $84 \times 20$  values of  $\hat{p}_i$  are distributed. In the histogram, the 95<sup>th</sup> percentile of  $\min(\hat{p}_i, 1 - \hat{p}_i)$  is around 0.1, and only 5% of  $\min(\hat{p}_i, 1 - \hat{p}_i)$  is larger than 0.1, which corresponds to only one element when  $n = 20$ .

We exploit this highly concentrated distribution of  $\hat{p}_i$  to aggressively short-circuit an exhaustive sum (10). In so doing, we obtain a reasonable approximation because it can be shown that  $\hat{p}(\mathbf{Z})$  quickly goes to a zero for  $\mathbf{Z} \in \mathcal{B}_r(\hat{\mathbf{Z}})$  as  $r$  increases. For example, suppose  $r = 1$ . For  $\mathbf{Z} \in \mathcal{B}_1(\hat{\mathbf{Z}})$ , let  $j$  denote the index of an element with  $Z_j \neq \hat{Z}_j$  and  $\min(\hat{p}_j, 1 - \hat{p}_j)$  within the 95<sup>th</sup> percentile. Then, we have

$$\hat{p}(\mathbf{Z}) = \hat{p}(\hat{\mathbf{Z}}) \frac{\min(\hat{p}_j, 1 - \hat{p}_j)}{\max(\hat{p}_j, 1 - \hat{p}_j)} \leq \frac{0.1}{1 - 0.1},$$

because  $\hat{p}(\hat{\mathbf{Z}}) \leq 1$  and  $\frac{\min(\hat{p}_j, 1 - \hat{p}_j)}{\max(\hat{p}_j, 1 - \hat{p}_j)} < 0.1 / (1 - 0.1)$ . The same holds more generally, for larger  $r$ , where  $\mathbf{Z} \in \mathcal{B}_r(\hat{\mathbf{Z}})$ :

$$\hat{p}(\mathbf{Z}) \leq \left( \frac{0.1}{1 - 0.1} \right)^r.$$

This value quickly decreases as  $r$  increases.

Since  $\hat{p}(\mathbf{Z})$  decreases exponentially as  $r$  increases, we can obtain a good approximation

to the exhaustive variance (10) by the truncated series,

$$\widehat{\text{Var}}_R[\mu_J(\mathbf{x}_*)] = \frac{\sum_{r=0}^R \sum_{\mathbf{z} \in \mathcal{B}_r(\hat{\mathbf{Z}})} s_J(\mathbf{x}_*; \mathbf{Z}) \hat{p}(\mathbf{Z})}{\sum_{r=0}^R \sum_{\mathbf{z} \in \mathcal{B}_r(\hat{\mathbf{Z}})} \hat{p}(\mathbf{Z})}. \quad (12)$$

This expression (12) approaches the true  $\text{Var}[\mu_J(\mathbf{x}_*)]$  as  $R \rightarrow n$ , requiring the evaluation of  $\sum_{r=0}^R \binom{n}{r}$  terms. When  $R = 0$ , the approximation in Eq. (12) reduces to  $s_J^2(\mathbf{x}_*; \hat{\mathbf{Z}})$ , which is a popular acquisition criteria in its on right, forming the basis of ALM (McKay et al. 2000), reviewed earlier in Section 1. Larger  $R$ -values yield only marginal gains, both in terms of the magnitude of the resulting variance estimate, and in terms of progress towards the true calculation. Again, looking ahead to our illustration coming next, our variance estimates, via Eq. (12) using  $R = 0$ , are within ten percent of the truth the truth (10), specifically 9.0181 and around 10, respectively. The former improves to 9.0194 with  $R = 1$ . We prefer  $R = 0$  for our empirical work later, although it’s certainly easy to try modestly larger  $R$ -values. Other implementation details are deferred to Section 5.

### 3.3 Accuracy of Bias and Variance

Here we validate the accuracy of the proposed bias and variance estimates empirically. We have found that their intricate form, complex cross-dependency across inputs, GP hyperparameter multiple plugin estimates, makes a theoretical analysis of their accuracy challenging. Instead, we meticulously design two simulated experiments to empirically assess how bias and variance estimates compare to their ground truth counterparts.

We use two test functions defined on a two-dimensional rectangular domain  $[-0.5, 0.5]^2$ , which are partitioned into four regions as illustrated in Figure 2. The response for each region is randomly drawn from an independent GP, each with distinct constant mean  $\mu_k \in \{0, 27, 54, 81\}$  and a squared exponential covariance function,

$$c(\mathbf{x}, \mathbf{x}'; \theta_k) = 9 \exp \left\{ -\frac{1}{200} (\mathbf{x} - \mathbf{x}')^T (\mathbf{x} - \mathbf{x}') \right\}.$$

Random realizations are taken on a regular 441 grid, among which we randomly select 120 values as training data, observed over independent Gaussian noise  $\mathcal{N}(0, 2^2)$ , for fitting a JGP and evaluating bias (9) and variance (12) the full grid. We repeat this process 25

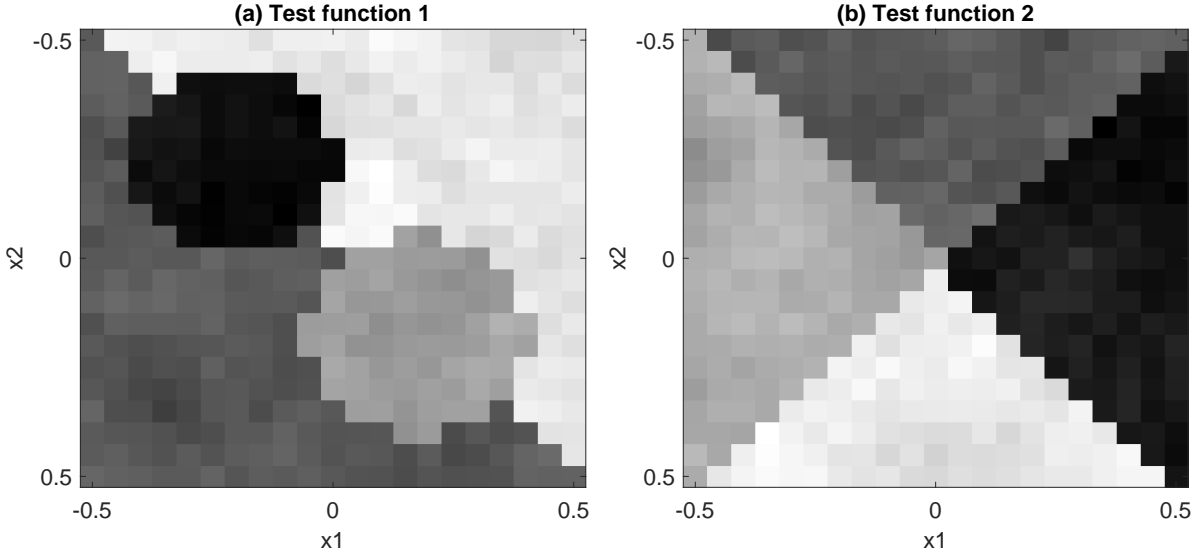


Figure 2: Test functions used to evaluate the bias and variances estimates.

times for each of the two test functions. To assess the accuracy of these estimates, we compare them with the theoretical bias and variance values derived from (19) and (10).

In our analysis of the results of this experiment, we studied the number of heterogeneous regions mixed in local data  $\mathcal{D}_n(\mathbf{x}_*)$  for each test location  $\mathbf{x}_*$ . This *degree-of-mix* is one when the test site is positioned well into interior a region, but the value be as high as four when it is near one or more borders. Recall that earlier we made the assumption of degree-2-of-mix to derive our bias estimate (19). We expect our bias estimate to be accurate when this assumption is valid. We are interested in checking this numerically, and we are also interested in checking how poor bias estimates can be when this assumption is not valid.

Figure 3 illustrates the differences between estimates and true values for four degree-of-mix groups. The bias estimates, displayed in the top panel, cluster around zero, but their variation increases as degree-of-mix rises. Examining the summary statistics in the plot titles, we find that for degree-of-mix values less than three, the average difference is close to zero, being significantly smaller than the true noise standard deviation of 2. This indicates high accuracy in bias estimation when degree-of-mix is less than three.

For larger degrees, the average difference is elevated but still remains below the noise standard deviation. However, observed variations of these differences increases significantly beyond a degree of two. This indicates a less well estimated bias. It's important to

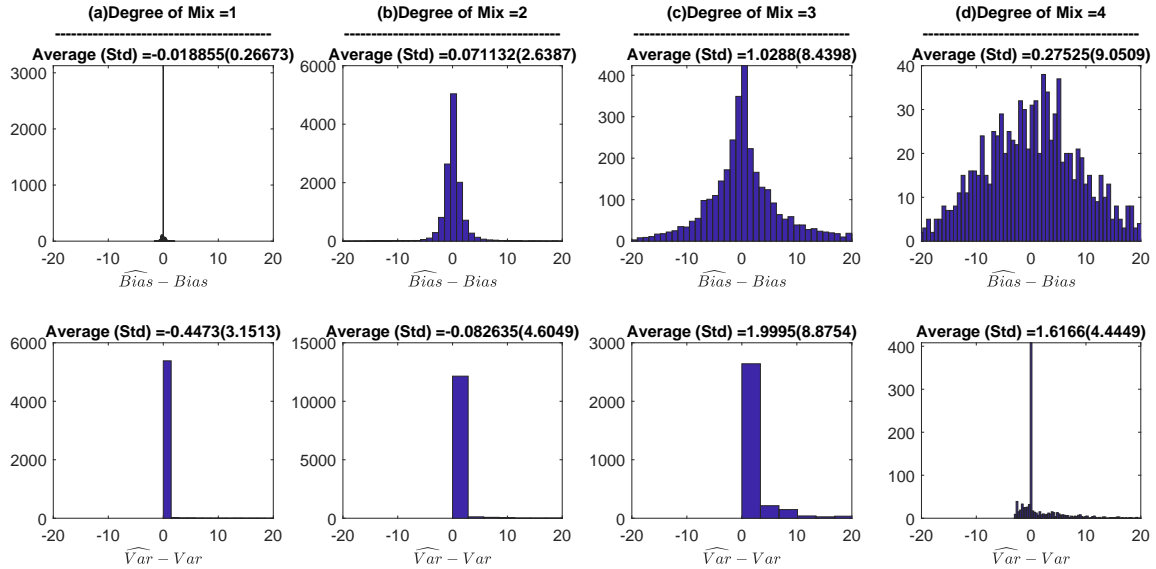


Figure 3: Difference of the bias and variances estimates from their true values.

note that these worst-case scenarios are rare: only 5% of the 22,050 test sites exhibit differences outside the  $\pm 3\sigma$  range. Moreover, we observed that the differences between the variance estimates and their true counterparts are slightly skewed positive, implying that the variances are underestimated. This happens because we use truncated series for our variance estimates (12). However, the degree of underestimation is low relative to the noise variance.

### 3.4 Illustration

Here we use a toy example to illustrate how the bias and variance of JGP estimates may be decomposed via the approximations laid out above. To ease visualization, we use a two-dimensional rectangular domain  $[-0.5, 0.5]^2$ , which is partitioned into two regions by a curvy boundary, as illustrated in Figure 4 (a). The response function for each region is randomly drawn from an independent GP with distinct constant mean  $\mu_k \in \{0, 27\}$  and a squared exponential covariance function,

$$c(\mathbf{x}, \mathbf{x}'; \theta_k) = 9 \exp \left\{ -\frac{1}{200} (\mathbf{x} - \mathbf{x}')^T (\mathbf{x} - \mathbf{x}') \right\}.$$

We added independent Gaussian noise  $\mathcal{N}(0, 2^2)$  to each response value.



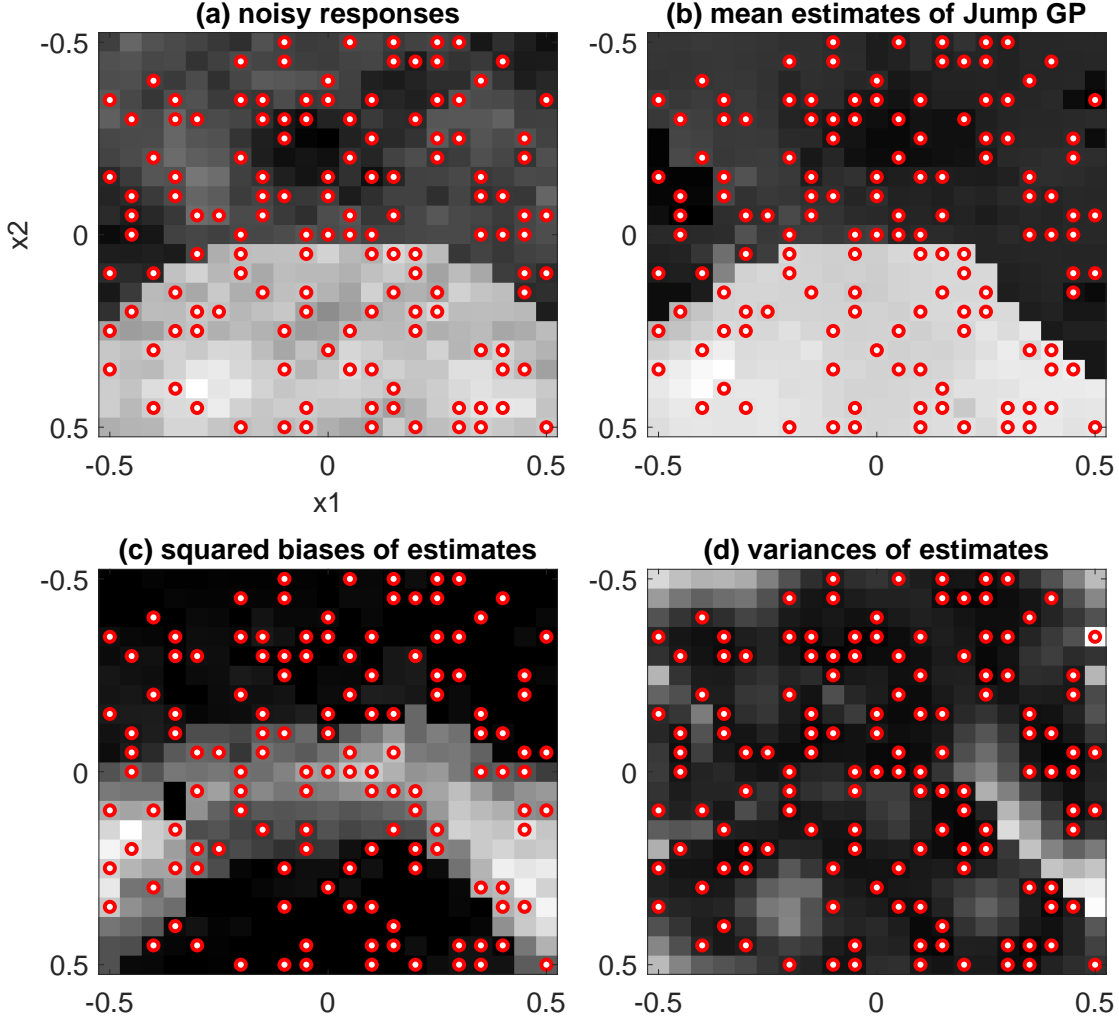


Figure 4: Bias and variances of JGP for a test function over a two-dimensional grid of  $(x_1, x_2)$  illustrated in (a). The red dots in all figures represent the training input locations. Panel (b) shows the mean estimates from JGP with the training data. Panels (c) and (d) show  $\widehat{\text{Bias}}[\mu_J(\mathbf{x}_*)]$  and  $\widehat{\text{Var}}_0[\mu_J(\mathbf{x}_*)]$  of the JGP estimates.

Figure 4 (a) shows a realization of one such surface. Overlaid are  $N = 132$  training inputs selected at random from a  $21 \times 21$  grid over the input domain. Noisy responses at those training inputs are used to estimate the JGP. Figure 4 (b) shows JGP-estimated predictive means over that grid. Figure 4 (c) and (d) show the decomposition of MSPE (7) via calculated values of  $\widehat{\text{Bias}}[\mu_J(\mathbf{x}_*)]$  and  $\widehat{\text{Var}}_0[\mu_J(\mathbf{x}_*)]$ , respectively. Observe in particular that high bias clusters around the boundary of the two regions, whereas high variance

clusters around parts of the input space where training data are sparse. The former is novel to the JGP setting, and a feature we intend to exploit next, for active learning. For JGP learning, you want more data where bias is high. The latter is a classic characteristic of (otherwise stationary) GP modeling; more data where training examples are sparse.

## 4 Active Learning for Jump GPs

Given training data  $\mathcal{D}_N = \{(\mathbf{x}_i, y_i), i = 1, \dots, N\}$ , we consider an AL setup that optimizes the acquisition of new training data by selecting a tuple of input coordinates  $\mathbf{x}_{N+1}$  among candidate positions in  $\mathcal{X}_C$ , of size  $N_C$ , according to some criterion. For all numerical examples in this paper, we take  $N_C = 100d$  and form  $\mathcal{X}_C$  via maximin LHD (Santner et al. 2003). Once  $\mathbf{x}_{N+1}$  has been selected, it is run to obtain  $y_{n+1} = f(\mathbf{x}_{n+1}) + \varepsilon$ , The training data is augmented to form  $\mathcal{D}_{N+1} = \mathcal{D}_N \cup (\mathbf{x}_{N+1}, y_{N+1})$ . Finally, the model is refit and the process repeats with  $N \leftarrow N + 1$ . Here we develop three AL criteria for JGPs that are designed account for predictive model bias variance to varying degree.

### 4.1 Acquisition functions

We first consider an ALM-type criterion, selecting  $\mathbf{x}_{N+1}$  where the MSPE (7) is maximized. Exploiting bias (9) and variance (12) estimates, we select  $\mathbf{x}_{N+1} \in \mathcal{X}_C$  as

$$\mathbf{x}_{N+1} = \operatorname{argmax}_{\mathbf{x}_* \in \mathcal{X}_C} \widehat{\text{MSPE}}(\mathbf{x}_*), \quad \text{where} \tag{13}$$

$$\widehat{\text{MSPE}}(\mathbf{x}_*) = \widehat{\text{Bias}}[\mu_J(\mathbf{x}_*)]^2 + \widehat{\text{Var}}[\mu_J(\mathbf{x}_*)].$$

We refer to this AL criteria as *Maximum MSPE Acquisition*.

Second, we explore an IMSPE (or ALC) type criterion that sequentially selects new data points among candidate locations in order to maximize the amount by which a new acquisition would reduce total variance throughout the input space. To evaluate how the MSPE of a JGP changes with a new data  $(\mathbf{x}_{N+1}, y_{N+1})$ , we must first understand how the addition of new training data affects the  $n$ -nearest neighbors of a test location  $\mathbf{x}_*$ .

Let  $R(\mathbf{x}_*) = \max_{\mathbf{x}_i \in D_n(\mathbf{x}_*)} d(\mathbf{x}_*, \mathbf{x}_i)$  denote the size of the neighborhood  $D_n(\mathbf{x}_*)$  before the new data is added, where  $d(\cdot, \cdot)$  is Euclidean distance in  $\mathcal{X}$  space. When  $d(\mathbf{x}_{N+1}, \mathbf{x}_*) \geq$

$R(\mathbf{x}_*)$ , the neighborhood does not change with the injection of the new data. Therefore, the change in MSPE would be zero at  $\mathbf{x}_*$ . Consequently, we only consider test locations  $\mathbf{x}_*$  satisfying  $d(\mathbf{x}_{N+1}, \mathbf{x}_*) < R(\mathbf{x}_*)$  going forward. Let  $\mathcal{X}(\mathbf{x}_{N+1})$  represent all test locations satisfying that condition. For  $\mathbf{x}_* \in \mathcal{X}(\mathbf{x}_{N+1})$ , let  $\mathcal{D}_n(\mathbf{x}_*, \mathbf{x}_{N+1})$  represent the new  $n$ -nearest neighborhood of  $\mathbf{x}_*$ . Without loss of generality, consider  $\mathbf{x}_{n,*} = \operatorname{argmax}_{\mathbf{x}_{i,*} \in \mathcal{D}_n(\mathbf{x}_*)} \|\mathbf{x}_* - \mathbf{x}_{i,*}\|$ . Then, we can write

$$\mathcal{D}_n(\mathbf{x}_*; \mathbf{x}_{N+1}) = \mathcal{D}_n(\mathbf{x}_*) \cup \{(\mathbf{x}_{N+1}, y_{N+1})\} - \{(\mathbf{x}_{n,*}, y_{n,*})\}. \quad (14)$$

When  $(\mathbf{x}_{N+1}, y_{N+1})$  are known, one can fit JGP to  $\mathcal{D}_n(\mathbf{x}_*; \mathbf{x}_{N+1})$ . Let  $\mu_J(\mathbf{x}_* | \mathbf{x}_{N+1}, \mathbf{y}_{N+1})$  and  $s_J(\mathbf{x}_* | \mathbf{x}_{N+1}, \mathbf{y}_{N+1})$  denote the posterior mean and variance, based on (1). The corresponding MSPE can be achieved using (9) and (12). The corresponding MSPE is

$$\widehat{\text{MSPE}}(\mathbf{x}_* | \mathbf{x}_{N+1}, y_{N+1}) = \widehat{\text{Bias}}[\mu_J(\mathbf{x}_* | \mathbf{x}_{N+1}, y_{N+1})]^2 + \widehat{\text{Var}}[\mu_J(\mathbf{x}_* | \mathbf{x}_{N+1}, y_{N+1})]. \quad (15)$$

In an AL setting, however,  $y_{N+1}$  is unknown at the time that an acquisition decision is being made. To assess the potential value of it's input,  $\mathbf{x}_{N+1}$ , we propose to estimate  $y_{N+1}$ , via the posterior (predictive) distribution of  $y_{N+1}$  based on the original data around  $\mathbf{x}_{N+1}$ , i.e.,  $\mathcal{D}_n(\mathbf{x}_{N+1})$ . Specifically, for a JGP  $Y(\mathbf{x}_{N+1}) | \mathcal{D}_n(\mathbf{x}_{N+1})$  via Eq. (5) we have  $p(y_{N+1} | \mathcal{D}_n(\mathbf{x}_{N+1})) \equiv \mathcal{N}_1(\mu_J(\mathbf{x}_{N+1}), \sigma^2 + s_J^2(\mathbf{x}_{N+1}))$ .

IMSPE may then be defined as the average MSPE over  $\mathbf{x}_*$  and  $y_{N+1}$ ,

$$\widehat{\text{IMSPE}}(\mathbf{x}_{N+1}) = \int \int \widehat{\text{MSPE}}(\mathbf{x}_* | \mathbf{x}_{N+1}, \mu_J(\mathbf{x}_{N+1})) p(y_{N+1} | \mathcal{D}_n(\mathbf{x}_{N+1})) d\mathbf{x}_* dy_{N+1}. \quad (16)$$

For acquisition, we are primarily interested in how injecting  $\mathbf{x}_{N+1}$  into the design improves the IMSPE, which may be measured as

$$\Delta \widehat{\text{IMSPE}}(\mathbf{x}_{N+1}) = \int \Delta \widehat{\text{MSPE}}(\mathbf{x}_* | \mathbf{x}_{N+1}) d\mathbf{x}_*,$$

where  $\Delta \widehat{\text{MSPE}}(\mathbf{x}_* | \mathbf{x}_{N+1}) = \int \widehat{\text{MSPE}}(\mathbf{x}_* | \mathbf{x}_{N+1}, y_{N+1}) p(y_{N+1} | \mathcal{D}_n(\mathbf{x}_{N+1})) dy_{N+1} - \widehat{\text{MSPE}}(\mathbf{x}_*)$ . The term  $\Delta \widehat{\text{MSPE}}(\mathbf{x}_* | \mathbf{x}_{N+1})$  is non-zero only for  $\mathbf{x}_*$  satisfying  $d(\mathbf{x}_{N+1}, \mathbf{x}_*) < R(\mathbf{x}_*)$ . Let  $\mathcal{X}(\mathbf{x}_{N+1}) = \{\mathbf{x}_* \in \mathcal{X}, d(\mathbf{x}_{N+1}, \mathbf{x}_*) < R(\mathbf{x}_*)\}$  represent the set of such test locations. The improvement can be further refined to

$$\Delta \widehat{\text{IMSPE}}(\mathbf{x}_{N+1}) = \int_{\mathcal{X}(\mathbf{x}_{N+1})} \Delta \widehat{\text{MSPE}}(\mathbf{x}_* | \mathbf{x}_{N+1}) d\mathbf{x}_*.$$

Unfortunately, this integral is not available in a closed form, but we have found that it can be approximated accurately using Monte Carlo-based quadrature. First draw a finite number of  $\mathbf{x}_*$ 's, based on a minimax distance design or other space filling design. The size of the draws is denoted by  $N_*$ , which depends on the size of domain  $\mathcal{X}$ . We used  $N_* = 20 \times d$  for all synthetic examples with  $\mathcal{X} = [-0.5, 0.5]^d$ . For each  $\mathbf{x}_* \in \mathcal{X}(\mathbf{x}_{N+1})$ , draw i.i.d. samples of  $y_{N+1}$  from  $p(y_{N+1} | \mathcal{D}_n(\mathbf{x}_{N+1}))$  and refit the JGP for each draw of  $y_{N+1}$  to evaluate the integral in  $\widehat{\Delta\text{MSPE}}(\mathbf{x}_* | \mathbf{x}_{N+1})$ . In the actual implementation, we use one deterministic draw of  $y_{N+1}$  at the posterior predictive mean,  $\mu_J(\mathbf{x}_{N+1})$ , as a computational shortcut. Finally, repeat to accumulate averages of  $\widehat{\Delta\text{MSPE}}(\mathbf{x}_* | \mathbf{x}_{N+1})$  to approximate  $\widehat{\Delta\text{IMSPE}}(\mathbf{x}_{N+1})$ . Selecting  $\mathbf{x}_{N+1} = \operatorname{argmin}_{\mathbf{x}_* \in \mathcal{X}_C} \widehat{\Delta\text{IMSPE}}(\mathbf{x}_{N+1})$  in this way yields what we dub a *Minimum IMSPE Acquisition*.

Our final AL criteria is *Maximum Variance Acquisition*

$$\mathbf{x}_{N+1} = \operatorname{argmax}_{\mathbf{x}_* \in \mathcal{X}_C} \widehat{\text{Var}}[\mu_J(\mathbf{x}_*)]. \quad (17)$$

Like the first criteria, above, this is an ALM-type, but one which ignores predictive bias. Focusing exclusively on variance which is known to produce space-filling designs. Consequently, it serves as a straw-man, or baseline in order to calibrate our empirical experiments and illustrations against a sensible benchmark.

## 4.2 Illustration

Here we use a simple toy example to explore the three acquisition functions presented in the previous section. For effective visualization, we use a two-dimensional rectangular domain  $[-0.5, 0.5]^2$ . In Figure 5 (a) this domain is partitioned into two regions,  $\mathcal{X}_1$  (lighter shading) and  $\mathcal{X}_2$  (darker). The noisy response function for each region is randomly drawn from an independent GP with the same regional means and covariance functions used in our Section 3.4 illustration plus additive independent Gaussian noise with  $\sigma = 2$ . AL is initialized with thirty seed-data positions via LHD, and these are overlaid onto all panels of the figure. Given noisy observations at these seed positions, we evaluated our three AL criteria on a  $21 \times 21$  grid of candidates  $\mathcal{X}_C$  in the input domain. Please note that  $X_C$  more densely locates for this demonstration to better visualize the criteria on the

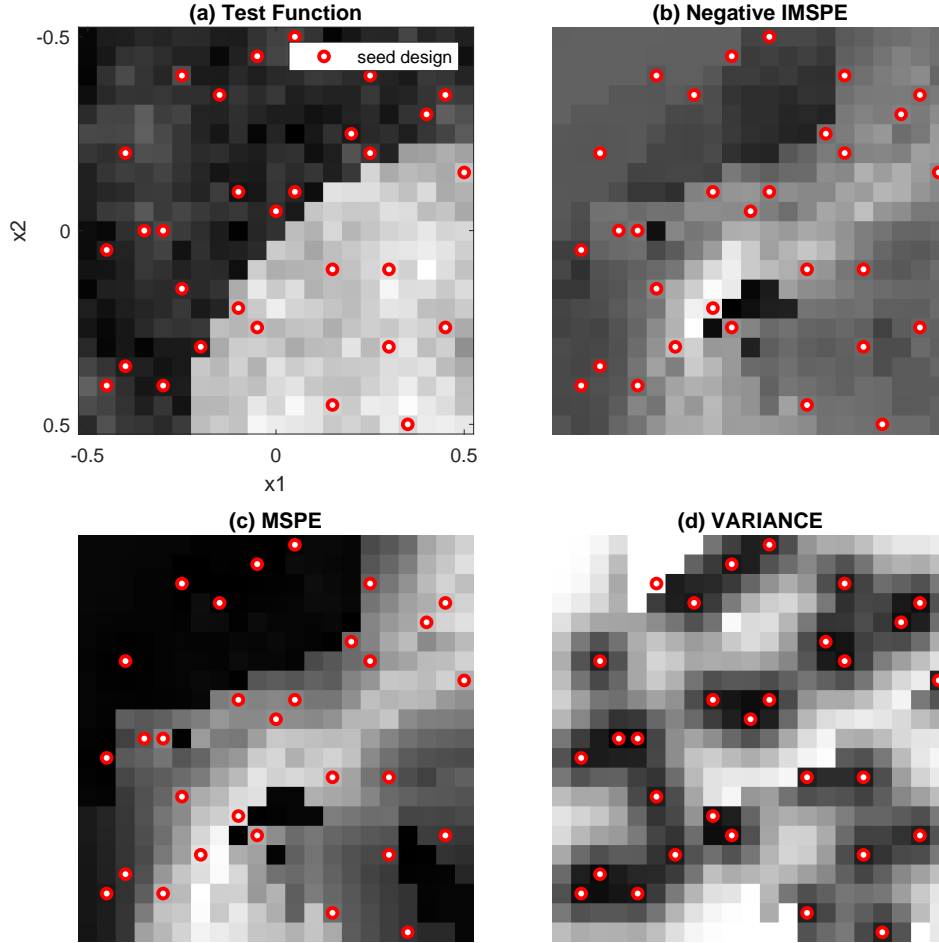


Figure 5: Three acquisition functions evaluated over  $21 \times 21$  grid locations on  $[-0.5, 0.5]^2$ . Panel (a) shows the data. Panels (b)-(d) show  $-\widehat{\text{IMSPE}}(\mathbf{x}_*)$ ,  $\widehat{\text{MSPE}}(\mathbf{x}_*)$  and  $\widehat{\text{Var}}[\mu_J(\mathbf{x}_*)]$ , respectively.

dense grid. Figure 5 (b)–(d) provides visuals for their values in greyscale. For example, the maximum variance criterion in (d) indicates  $\widehat{\text{Var}}[\mu_J(\mathbf{x}_*)]$ . Observe that this criteria is inversely proportional to the positions (and densities, locally) of the seed data. This criteria exhibits behavior similar to conventional variance-based criteria (such as ALM or ALC) derived from stationary GPs. One slight difference, however, is that that the variance of JGP is slightly higher around regional boundaries, compared to an ordinary stationary GP. Around the boundaries, local data is bisected, and only one section is used for JGP prediction, which makes the variance elevated around the boundaries. Later, in Figure 6,

we will see that slightly more data positions are selected around regional boundaries with the variance criterion. As shown in panels (b) and (c), the negative IMSPE and MSPE values consider model bias and variance. Around regional boundaries, bias values dominate variance estimates. Therefore, as we will show in Figure 6, data acquisitions are highly concentrated around regional boundaries.

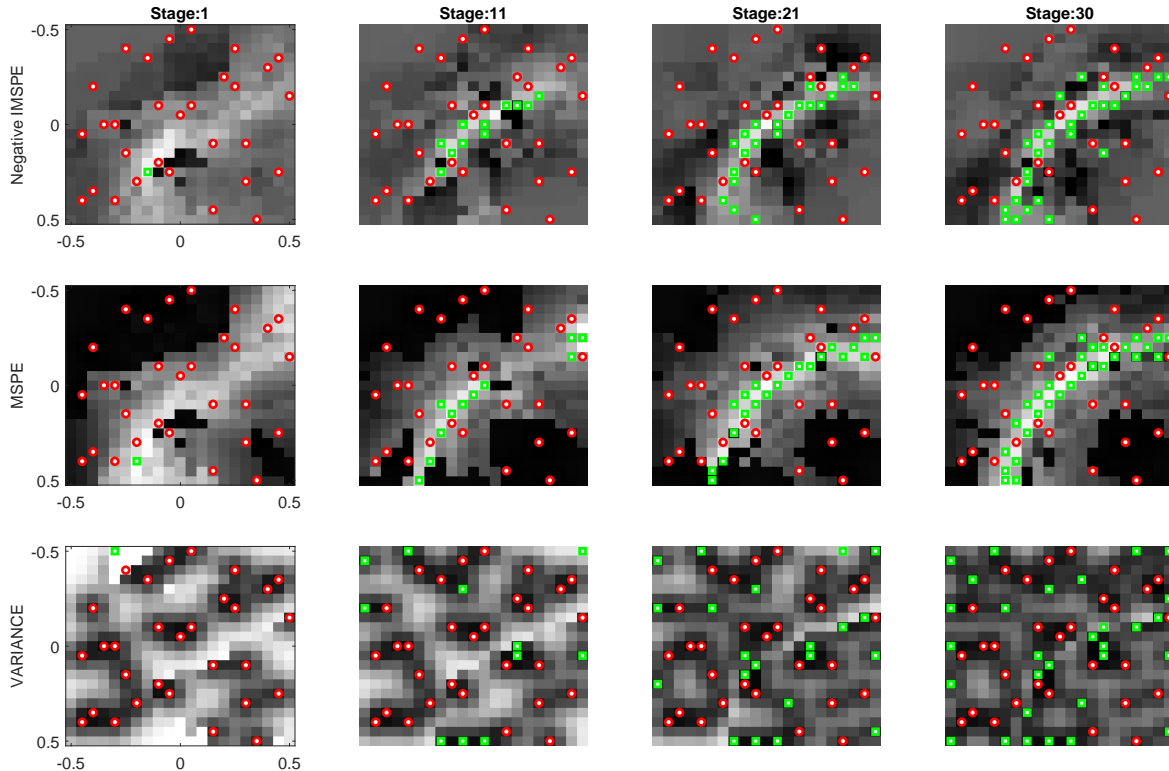


Figure 6: Active selection of design points for three acquisition functions. Dots represent seed designs, and boxes represent the design points added by active learning.

Future acquisitions further differentiate themselves according to the heuristic in question. For the same toy example, we ran AL for each choice of the three acquisition functions: start with a seed design of 30 random LHD data points; subsequently add one additional design point every AL stage for 30 stages. Figure 6 shows how the acquisition function values change as the AL stages progress and how they affect the selection training data inputs. For the IMSPE and MSPE criteria, the selected positions are highly concentrated around regional boundaries. With the variance criterion, the positions are close to a uniform distribution with a mild degree of concentration around the regional boundary.

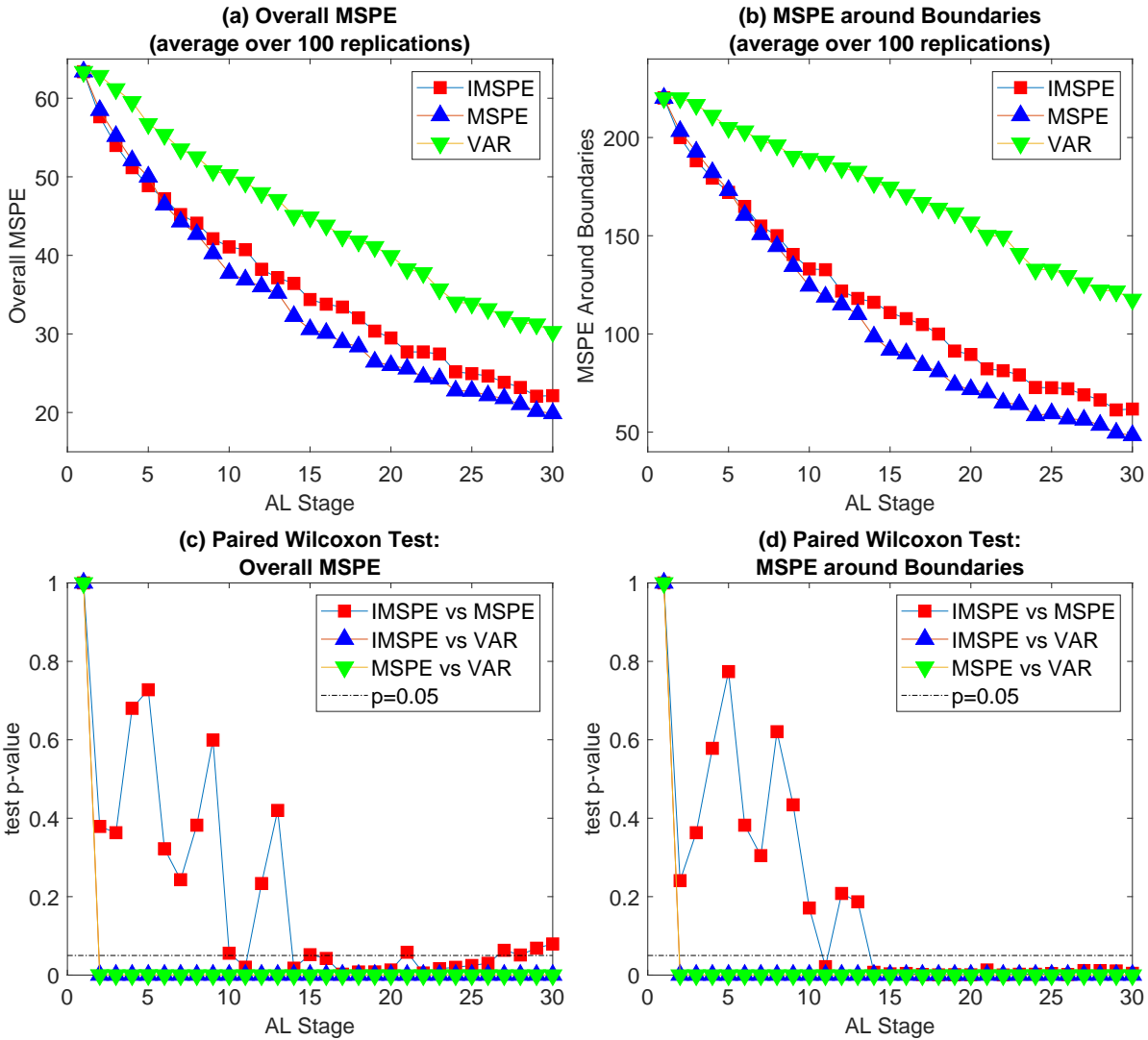


Figure 7: MSPE of JGP for different stages of active learning. The top panels show the average MSPE over 100 replicated experiments. The bottom panels show the p-values of the paired Wilcoxon test for statistical significance.

To explore accuracy of JGP under these three AL regimes, we conducted the Monte Carlo experiment in 100 replications. Each of these follows the same format as above, augmented to track JGP out-of-sample MSPE along the way in two variations. The first involves a testing set comprising of the 441 locations on the  $21 \times 21$ ; the second contains only the 82 closest of those locations to the regional boundary. We also performed a paired Wilcoxon test to determine if any performance differences were statistically significant

across Monte Carlo reps.

The top row of the figure shows overall MSPE, whereas the bottom row shows  $p$ -values from the Wilcoxon tests(s). The left column of panels use the full predictive grid, whereas focus on the regional boundary. It is clear from the top row that IMSPE and MSPE-based designs eventually outperform VAR, whereas the bottom row shows that the distinctions between the methods is more pronounced in early acquisitions, and that there is no difference (statistically speaking) between IMSPE and MSE. Since MSPE is faster (IMSPE averaged 0.12 seconds per acquisition, versus 0.07 seconds for MSPE), we generally prefer this simpler variation going forward.

## 5 Empirical benchmarking and validation

In this section, we use simulation experiments and two real experiments to validate the proposed AL strategies for the JGP. Our metrics include out-of-sample mean root squared error (RMSE, smaller is better) and the negative log posterior score (Gneiting & Raftery 2007, Eq. 25), which is proportional to the predictive Gaussian log likelihood (NLPD, smaller is better). We check how the two criteria change as more data are injected via AL.

We compare the four proposed criteria, JGP/MSPE, JGP/IMSPE, JGP/ALC and JGP/VAR, with benchmark methods. The first baseline benchmark is the stationary GP with the ALC criterion, labeled as GP/ALC. We also considered an existing non-stationary GP model and its associated ALC criterion: Treed GP/ALC (Gramacy & Lee 2008), which is the best performer among it and two-layer Deep GP/ALC (Sauer et al. 2020). The two-layer Deep GP/ALC did not perform very good for the experiments we performed with small data sizes, because the Deep GP is better suited for large data sizes. For the Treed GP/ALC, we use the `tgp` package (Gramacy & Taddy 2016). Our implementation of the JGP, and the associated AL subroutines introduced in this manuscript, may be downloaded from the author’s website: <https://www.chiwoopark.net/code-and-dataset>. Here too we use the defaults suggested by the software documentation. For example, we set the local data size to  $n = 15$ .

We first describe the benchmark datasets in Section 5.1. We compare the performance of the four proposed criteria on the benchmark datasets in Section 5.2. We perform the



comparison of JGP/MSPE and JGP/ALC with GL/ALC and Treed GP/ALC in Section 5.3. We intentionally have the two separate comparison sections, because the RMSE values of JGP, GP and Treed GP are very different, and squeezing them into the same comparison plots does not show clear distinctions among closer performers. In Section 5.3, we include JGP/MSPE as the best performer among the four proposed criteria and also include JGP/ALC to show the difference due to different surrogate choices with the same active learning strategies.

## 5.1 Benchmark Datasets

We use various simulated datasets and two real datasets summarized below:

**Bi-mixture GP datasets (BGP)**,  $d = 2, 3, 4, 5$ . We first work with synthetic examples in a rectangular domain  $[-0.5, 0.5]^d$  of varying dimension. The test functions are randomly sampled from a two-region partitioned GP model

$$f(\mathbf{x}) = f_1(\mathbf{x})1_{\mathcal{X}_1}(\mathbf{x}) + f_2(\mathbf{x})1_{[0,1]^d \setminus \mathcal{X}_1}(\mathbf{x}),$$

where  $\mathcal{X}_1 = \{\mathbf{a}^T \mathbf{x} \geq 0\}$  with  $\mathbf{a}$  chosen uniformly at random in  $\{-1, 1\}^d$ ,  $f_1$  drawn from a zero-mean GP with variance 9, and the isotropic Gaussian correlation function with length scale  $0.1 \times d$ , and  $f_2$  from a GP with mean 13, variance 9, and correlation function identical to  $f_1$ . Observations were then simulated independent Gaussian noise with variance 4.

**Smart factory dataset (SMF)**,  $d = 4$ . Figure 8 (a) depicts an automated material handling system (AMHS) in a semiconductor manufacturing facility (fab). The AMHS employs autonomous vehicles that run on overhead rails to optimize material flow and transfer silicon wafers between wafer fabrication steps. The AMHS aims to maintain high delivery speeds and keep low levels of human-related intervention and contamination. It has been observed that the AMHS becomes a major bottleneck in the fabrication process as the wafer production level increases (Siebert et al. 2018). Fab operators widely use simulation to optimize design and operational policies under various AMHS operating scenarios (Kang et al. 2022). Here we use a high-fidelity computer simulation model to evaluate the performance of AMHS under various design configurations. The simulation consists of 200

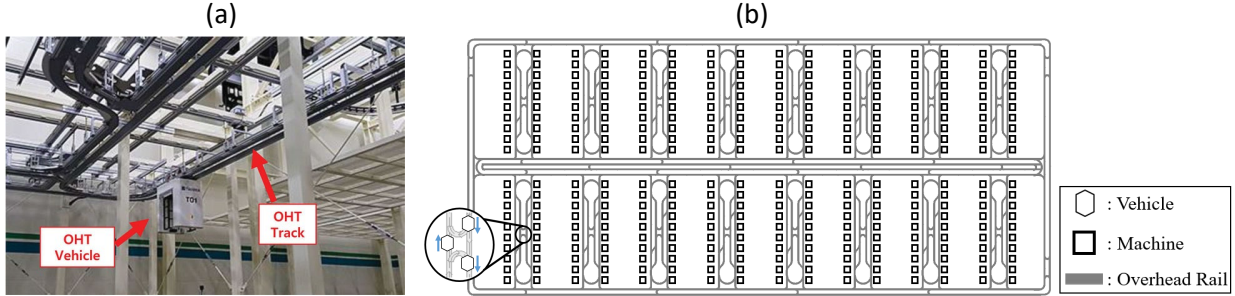


Figure 8: Simulated layout of automated material handling system. Part (a) is a reprint of Hwang & Jang (2020, Figure 1) under License CC BY-NC-ND 4.0.

autonomous vehicles running on the layout of overhead rails depicted diagrammatically in Figure 8 (b).

A key performance metric associated with AMHS is the waiting time until an autonomous vehicle is finally assigned to serve a transfer request. Since the relationship between vehicle specifications and the performance metrics is of great interest (Yang et al. 1999), we consider three design variables regarding vehicle specifications that are thought to affect this waiting time: vehicle acceleration, vehicle speed, and the required minimum distance between vehicles. We also consider one operational design variable: the maximum search range of empty vehicles in a distance-based vehicle dispatching policy. The policy aims to reduce the mean and variation of empty travel time. It is desirable to optimize the maximum search range of empty vehicles by controlling the trade-off between the idle time and empty travel time of vehicles. These design variables and sensible ranges are summarized in Table 1.

Design Variables	Minimum	Maximum
vehicle acceleration (meters/second <sup>2</sup> )	0.25	5.0
vehicle speed (meters/second)	2.5	3.5
required minimum distance between vehicles (meters)	0.25	1
maximum search range of empty vehicles (meters)	30	500

Table 1: Design variables for AMHS simulations.

Preliminary experiments revealed that transfer waiting times are almost zero under

most normal operating conditions, but can suddenly jump to significant levels as those conditions transition into “heavy traffic” situations. We posit that JGP with AL is a suitable approach to learn these jumping behaviors. We also observe from the preliminary study that the response variable of this example is split into regions by linear boundaries aligned to some coordinate directions. This regime change can only effectively modeled by JGP and TGP.

**Carbon nanotube yield dataset (CNT),  $d = 2$ .** Here we present an application of the proposed JGP-AL strategy to a materials research problem, illustrating the applicability of the new approach. Due to high experimental expense, we can only illustrate how the new approach is applied to this real application.

Our colleagues at the Air Force Research Lab (AFRL) developed an autonomous research experimentation system (ARES) for carbon nanotubes (Nikolaev et al. 2016). ARES is a robot capable of performing closed-loop iterative materials experimentation, carbon nanotube processing and ultimately measuring in-line process yield. Here, we utilize ARES to map out carbon nanotube yields as a function of two input conditions: reaction temperature and the log ratio of an oxidizing chemical concentration and a reducing chemical concentration. In previous experiments it was observed that nanotube yields are almost zero in certain growth conditions. Then suddenly, when those conditions approach a regime where they become more activated, yield “jumps” up to a substantial level. These activating conditions vary significantly depending on how the two inputs we varied.

## 5.2 Empirical evaluation

For the BGP and SMF, we set the seed design size to  $N = 20 \times d$  and the number of the AL stages to 50. The second real dataset originates from chemical experiments, and due to experimental expenses, we were unable to conduct as many experiments as in other cases. Our experimentation system is designed to run multiple experiments in parallel, making it amenable to active learning (AL) in batches. We began with a set of  $N = 20$  seed experiments, via LHD, and sequentially added batches of three new runs over five AL stages. Selection of each batch was performed by iteratively deploying single-point

acquisition, followed by imputing the missing output with the predictive mean furnished by the JGP.

Figures 9 and 10 depict the trend of the RMSE and NLPD values as the active learning stages progress. For the simulated BGP datasets, we average the values over 50 Monte Carlo (MC) replications, while for the remaining datasets, the values are based on one experimental campaign. Tables 2 and 3 present the statistical significance of the comparison for the BGP datasets, using paired Wilcoxon tests. The tables display the  $p$ -values for pairwise comparisons. The comparison reveals that incorporating bias into the design of active learning criteria significantly enhances the accuracy of JGP. Specifically, for the BGP and SMF datasets, JGP/MSPE—created by adding the bias term to JGP/VAR—outperforms JGP/VAR, which only considers the variance term.

For the CNT dataset, JGP/MSPE and JGP/VAR exhibit similar performance with comparable choices of design points. To further investigate, we examined the bias and variance estimates of JGP for this dataset. We discovered that the variance values are significantly larger than the squared bias values. Consequently, both JGP/MSPE and JGP/VAR have a similar ability reduce variance with acquisitions. This does not imply that both of them lead to a space-filling design, unlike the variance-based AL criterion of the stationary GP. As we illustrated in Section 4.2, The JGP/VAR selects distinct designs compared to GP/ALC, as it tends to concentrate more around the regional boundaries. Figure 11 confirms this with the CNT example, as the design points selected by JGP/VAR have concentrations around the regional boundaries.

p-values	BGP $d = 2$	BGP $d = 3$	BGP $d = 4$	BGP $d = 5$
JGP/IMSPE vs JGP/ALC	0.0000	0.0025	0.0007	0.0057
JGP/MSPE vs JGP/VAR	0.0000	0.0067	0.0000	0.0747
JGP/IMSPE vs JGP/MSPE	0.8810	0.0000	0.0000	0.0000
JGP/IMSPE vs JGP/LHD	0.0000	0.0000	0.0103	0.0003
JPG/MSPE vs JGP/LHD	0.0000	0.9346	0.0000	0.1778

Table 2: Statistical significance of the performance comparison of JGP/ALC, JGP/IMSPE, JGP/VAR, JGP/MSPE, and JGP/LHD, based on paired Wilcoxon tests with RMSE

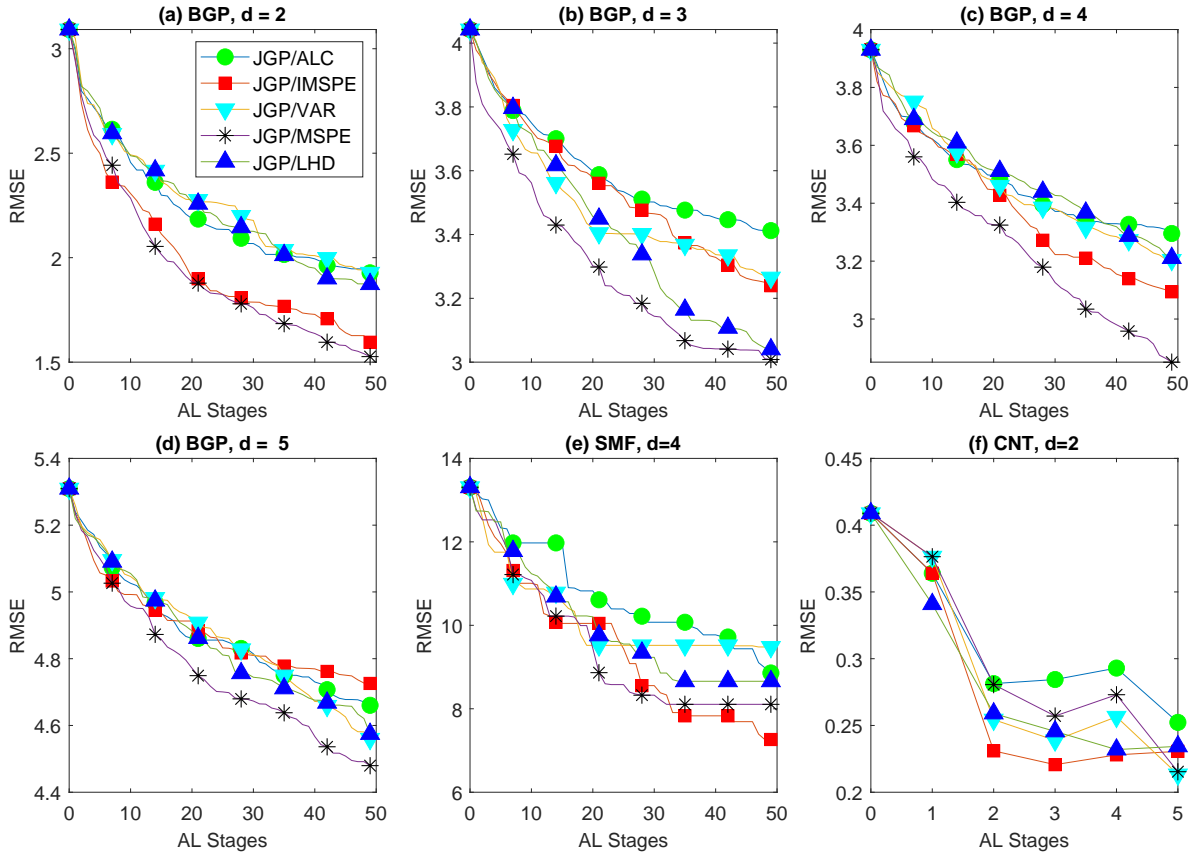


Figure 9: RMSE of JGP/ALC, JGP/IMSPE, JGP/VAR, JGP/MSPE, and JGP/LHD. Plots (a) to (d) values reported are based on 50 MC repetitions. Plot (f) is based on a batch active learning with three experiments per each AL stage.

Another intriguing comparison involves JGP/MSPE, JGP/IMSPE, and JGP/LHD. The first two are based on active learning strategies, while the last relies on a simple space-filling design. In simulated cases, both JGP/IMSPE and JGP/MSPE outperform JGP/LHD with statistically significant margins, except for the BGP dataset with  $d = 3$ . Additionally, JGP/IMSPE and JGP/MSPE outperform JGP/LHD for the SMF dataset. Notably, for the CNT dataset, JGP/IMSPE achieves a faster RMSE convergence to the bottom level compared to JGP/LHD, along with significantly lower NLPD values

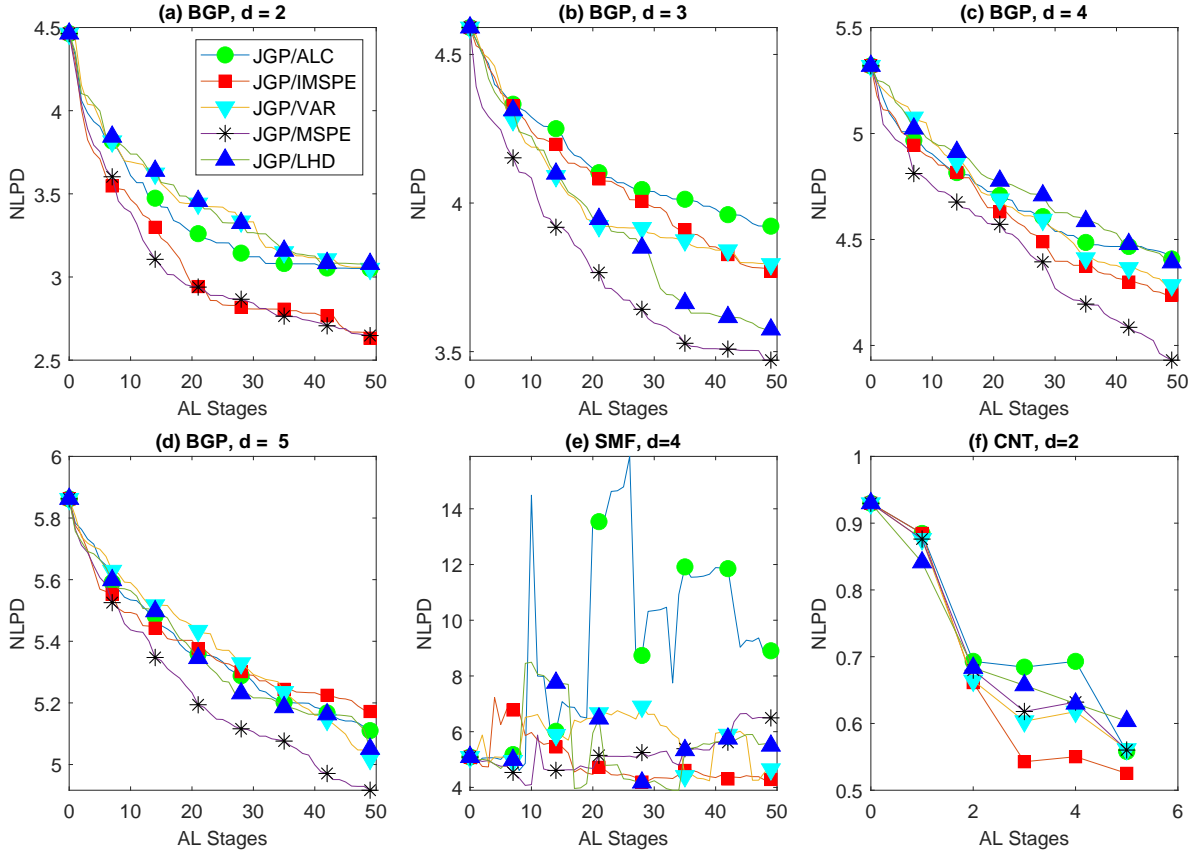


Figure 10: NLPD of JGP/ALC, JGP/IMSPE, JGP/VAR, JGP/MSPE, and JGP/LHD. Plots (a) to (d) values reported are based on 50 MC repetitions. Plot (f) is based on a batch active learning with three experiments per each AL stage.

### 5.3 Comparison to Treed GP and Stationary GP

We compare the best performers among the proposed AL criteria—JGP/MSPE and JGP/IMSPE—with TGP/ALC and GP/ALC. We like to note that the compared approaches are not only different in their active learning criteria but also different in their modeling approaches, so the differences in RMSE and NLPD metrics are not purely due to the choices of training data. Throughout this comparison, we aim to demonstrate that JGP with the an AL criteria that incorporates bias has a better capability of learning piecewise continuous surrogates than other non-stationary and stationary models.

Figures 12 and 13 show the trends of RMSE and NLPD as AL progresses for the

p-values	BGP $d = 2$	BGP $d = 3$	BGP $d = 4$	BGP $d = 5$
JGP/IMSPE vs JGP/ALC	0.0021	0.3413	0.2815	0.0882
JGP/MSPE vs JGP/VAR	0.0000	0.0001	0.0006	0.2729
JGP/IMSPE vs JGP/MSPE	0.5269	0.0000	0.0115	0.0000
JGP/IMSPE vs JGP/LHD	0.0000	0.0000	0.0004	0.0440
JGP/MSPE vs JGP/LHD	0.0000	0.4255	0.0000	0.0053

Table 3: Statistical significance of the performance comparison of JGP/ALC, JGP/IMSPE, JGP/VAR, JGP/MSPE, and JGP/LHD, based on paired Wilcoxon tests with NLPD

six test cases; Tables 4 and 5 show the results of the pairwise Wilcoxon tests on RMSE and NLPD. Observe that two non-stationary models outperform GP/ALC significantly in RMSE and NLPD for all of the six test cases. This demonstrates the advantage of using nonstationary GP models versus the conventional stationary GP model for data from these particular processes. It is also interesting to note that JGP/MSPE and JGP/IMSPE outperform TGP/ALC with significant margins in RMSE for the simulated BGP datasets and the CNT dataset. For those datasets, TGP/ALC perform more closely to GP/ALC. This can be understood through illustration in Figure 14, which shows the AL-based design selections for the CNT dataset. The TGP/ALC selects design points similarly as GP/ALC. For the SMF dataset, JGP/MSPE and JGP/IMSPE perform comparably to TGP/ALC. As we noted in the data description, the SMF process undergoes regime changes along coordinate-wise directions, for which the TGP model is perfectly suited.

p-values	BGP $d = 2$	BGP $d = 3$	BGP $d = 4$	BGP $d = 5$
JGP/IMSPE vs TGP/ALC	0.0000	0.0000	0.0000	0.0000
JGP/MSPE vs TGP/ALC	0.0000	0.0000	0.0000	0.0000
JGP/IMSPE vs GP/ALC	0.0000	0.0000	0.0000	0.0000
JGP/MSPE vs GP/ALC	0.0000	0.0000	0.0000	0.0000

Table 4: Statistical significance of the performance comparison of JGP/IMSPE, JGP/MSPE, TGP/ALC and GP/ALC, based on paired Wilcoxon tests with RMSE

NLPD results for JGP are not as good as via RMSE. At a few test locations, JGP

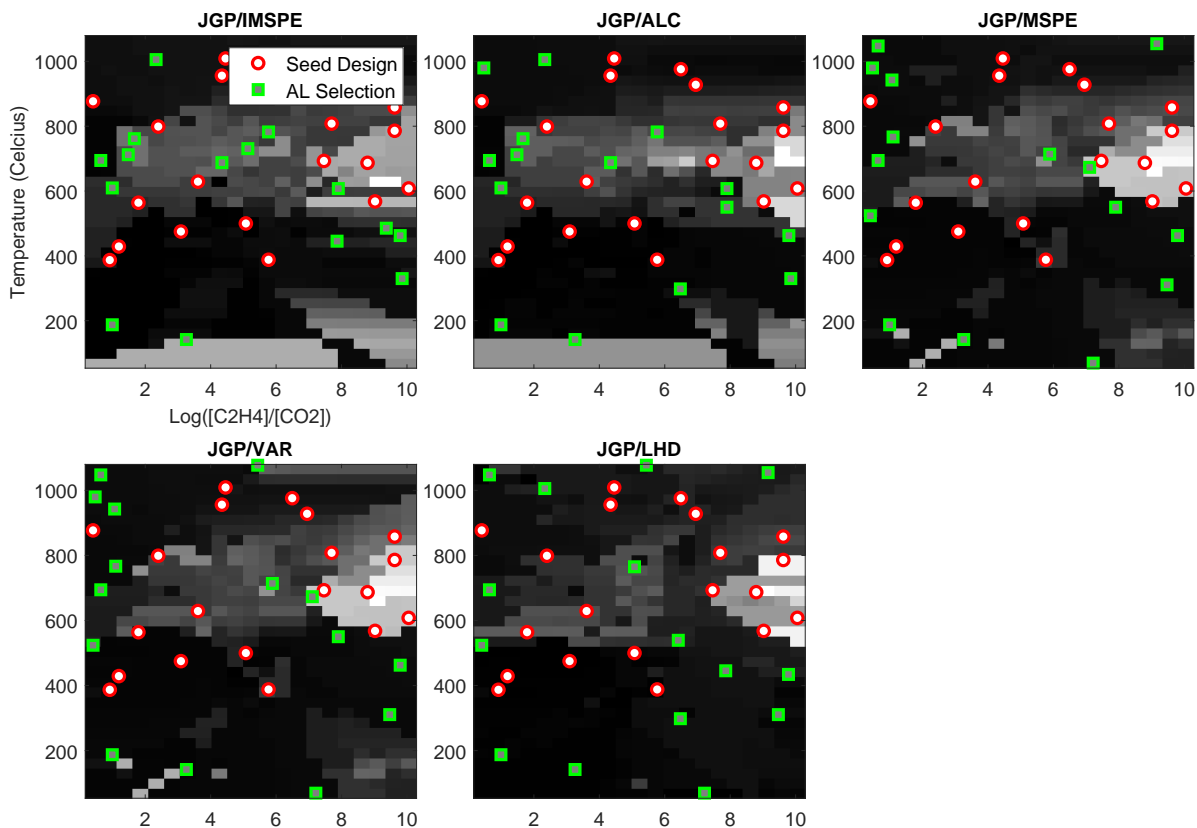


Figure 11: Active learning of JGP for the CNT dataset with the proposed criteria

produced very small predictive variance values, which makes the overall NLPD look much worse. For instance, in the SMF dataset example, only 2 out of 2069 test locations have predictive variance smaller than 0.0001. If we exclude these two cases, the NLPD of JGP becomes quite comparable to that of TGP. The underestimation of variance is primarily due to the local nature of JGP. In some test locations, hyperparameter learning with a small number of local data fails to yield accurate hyperparameters, resulting in underestimated variance estimates.



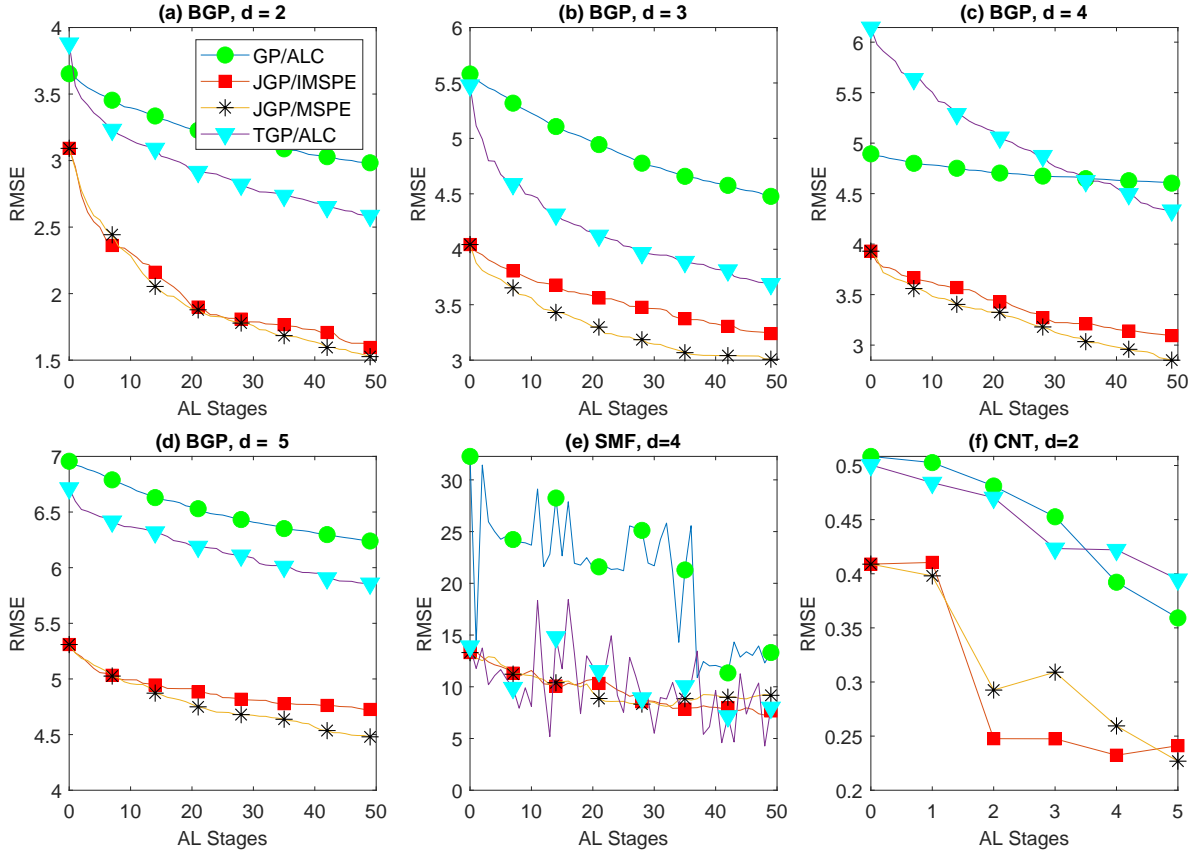


Figure 12: RMSE of JGP/IMSPE, JGP/MSPE, TGP/ALC and GP/ALC. Plots (a) to (d) values reported are based on 50 MC repetitions. Plot (f) is based on a batch active learning with three experiments per each AL stage.

## 6 Conclusion

We explored the Jump Gaussian process (JGP) model as a surrogate for piecewise continuous response surfaces. We studied estimates of predictive bias and variance for the JGPs with an eye toward developing an effective active learning (AL) heuristic for the model. We showed that JGP bias is largely influenced by the accuracy of the classifier governing regimes learned by the JGP, whereas model variance is comparable to that of the standard GP model. Consequently, to reduce model bias and variance together we should invest more data points (via AL) around boundaries between regimes, while otherwise continuing to place data points around less populated areas of a design space. Based on that principle, we

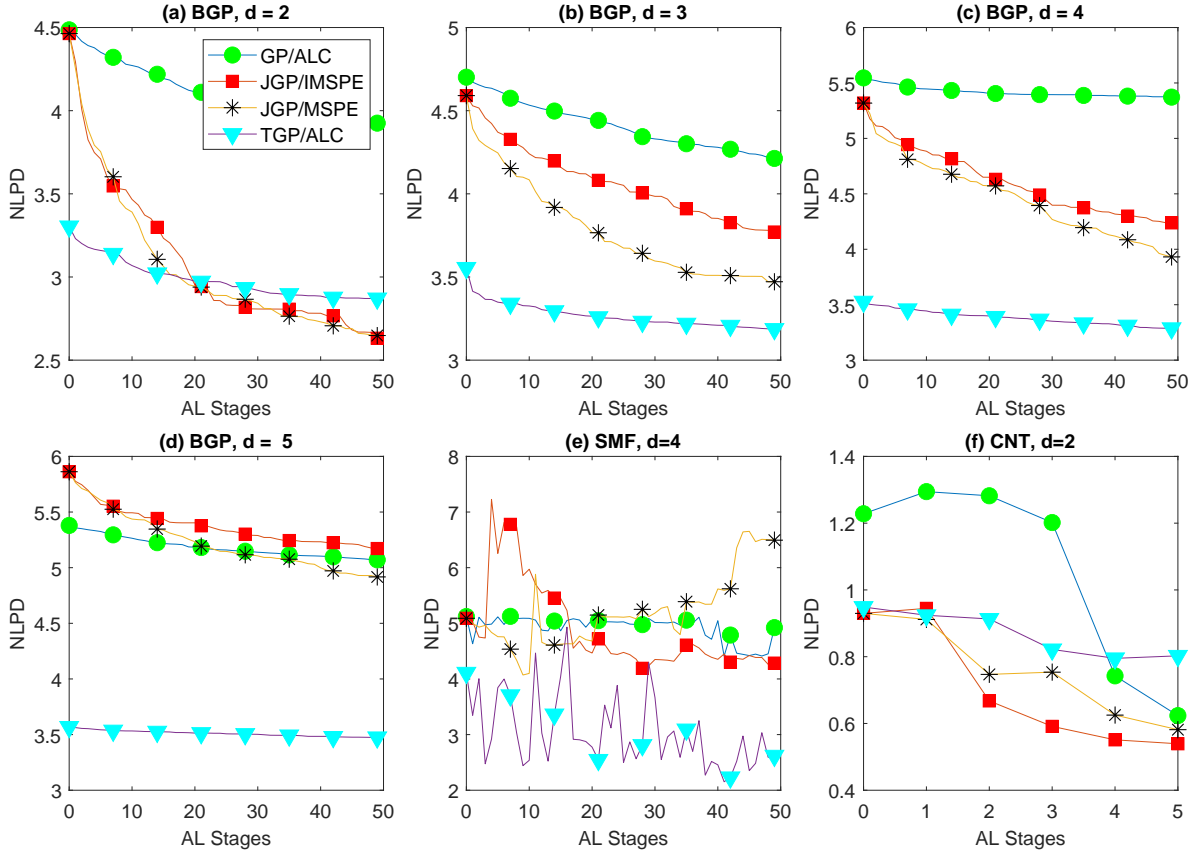


Figure 13: NLPD of JGP/IMSPE, JGP/MSPE, TGP/ALC and GP/ALC. Plots (a) to (d) values reported are based on 50 MC repetitions. Plot (f) is based on a batch active learning with three experiments per each AL stage.

introduced four AL criteria: one minimizing the integrated mean squared prediction error (JGP/IMSPE), another minimizing the integrated predictive variances (JGP/ALC), the third one placing points at the peak of the mean squared prediction error (JGP/MSPE), and the last one placing at the peak of the predictive variance (JGP/VAR).

We evaluated these four comparators using various simulation scenarios by tracking the changes in root mean square prediction error (RMSE) negative log posterior density (NLPD) and other metrics. Based on that evaluation, we determined that JGP/MSPE and JGP/IMSPE offered better AL performance than the purely variance-based criteria of JGP/ALC and JGP/VAR. We also compared JGP/MSPE and JGP/IMSPE criterion

p-values	BGP $d = 2$	BGP $d = 3$	BGP $d = 4$	BGP $d = 5$
JGP/IMSPE vs TGP/ALC	0.0000	0.0000	0.0000	0.0000
JGP/MSPE vs TGP/ALC	0.0000	0.0177	0.0340	0.0000
JGP/IMSPE vs GP/ALC	0.0000	0.0005	0.0000	0.1077
JGP/MSPE vs GP/ALC	0.0000	0.0000	0.0000	0.1938

Table 5: Statistical significance of the performance comparison of JGP/IMSPE, JGP/MSPE, TGP/ALC and GP/ALC, based on paired Wilcoxon tests with NLPD

to the stationary GP model with the ALC criterion and an existing non-stationary GP model and its associated ALC criterion, a Bayesian treed GP with ALC. The JGP and TGP outperformed GP, which shows the necessity of non-stationary models for the test scenarios. JGP outperformed TGP for most of the test cases, which shows the versatility of JGP over TGP for various non-stationary datasets.

Finally, we illustrated the applicability of our methods with two real experiments. Our first example involved a study of the performance of an autonomous material handling system in smart factory facilities. In the second experiment we highlighted a real materials design application of the proposed method for effectively mapping carbon nanotube yield as a function of two design variables. In this example, JGP/MSPE and JGP/IMSPE outperformed TGP and GP with a significant margin.

## Acknowledgment

We acknowledge support for this work. Park and Gramacy are supported by the National Science Foundation (NSF-2420358, NSF-2152679). Waelder and Maruyama are supported by the Air Force Office of Scientific Research (LRIR-19RXCOR040). Kang and Hong are partially supported by the National Research Foundation of Korea (NRF-2020R1A2C2004320) and by the BK21 FOUR of the National Research Foundation of Korea (NRF-5199990914451). The main algorithm of this work is protected by a patent pending with application number 18/532,296.

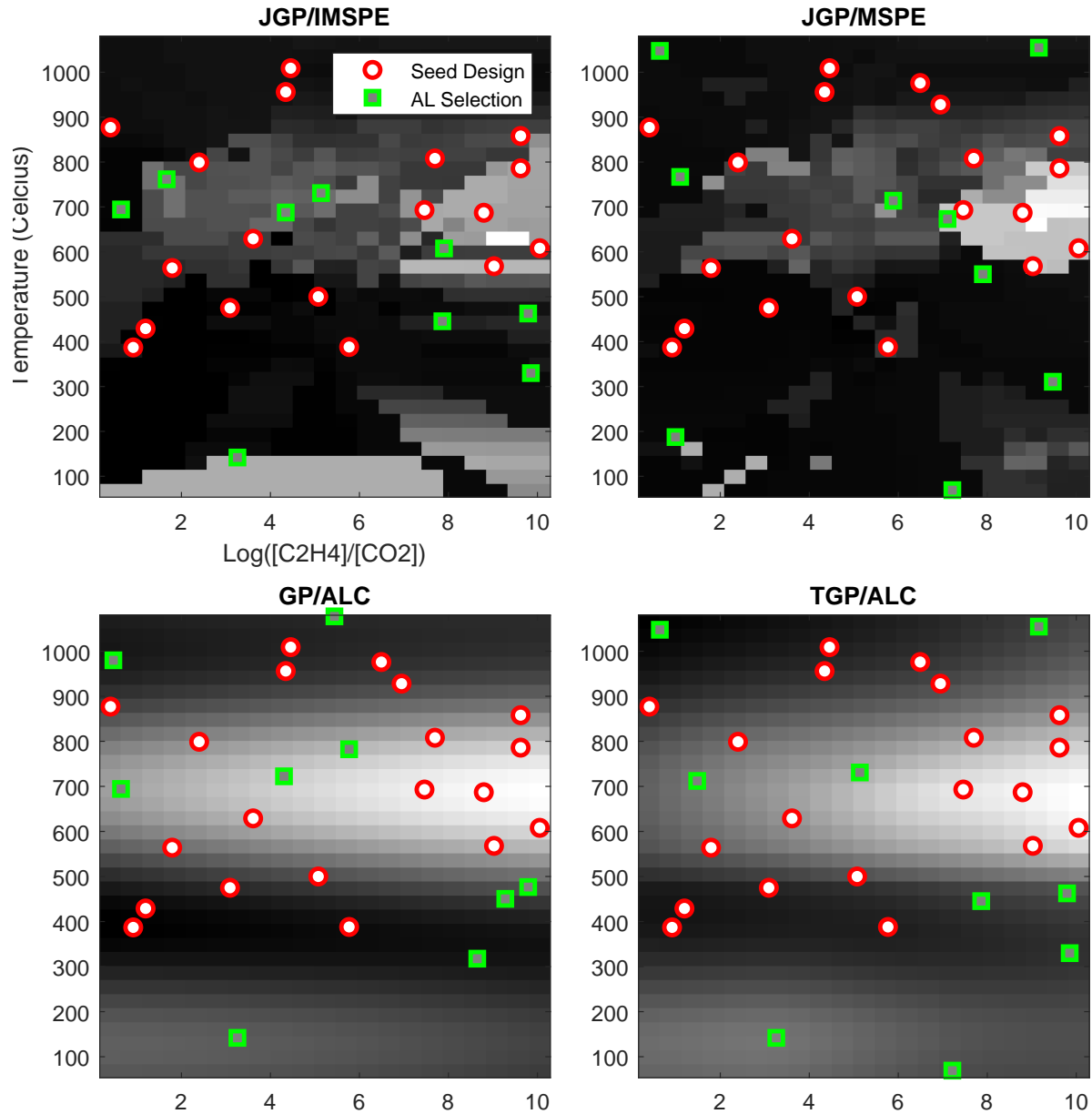


Figure 14: Active learning of JGP, GP and TGP for the CNT dataset. The results shown are obtained after the third AL stage when the compared approaches have shown biggest differences.

## Appendix A. Proof of Theorem 1

Begin by writing the JGP mean estimator  $\hat{m}_*$  in Eq. (6) as a dot product  $\hat{m} = \alpha y_*$ , where the  $i^{\text{th}}$  component of  $\alpha = (\alpha_1, \dots, \alpha_{n_*})$  is given as follows:

$$\alpha_i = \left( \frac{\mathbf{1}_{n_*}^T (\sigma^2 \mathbf{B}_{\mathcal{G}_*} + \mathbf{C}_{**})^{-1}}{\mathbf{1}_{n_*}^T (\sigma^2 \mathbf{I}_{n_*} + \mathbf{C}_{**})^{-1} \mathbf{1}_{n_*}} \right)_i.$$

With this notation, one may write  $\hat{m}_* = \sum_{i \in \mathcal{D}_{n,*}} \alpha_{i,*} y_{i,*}$ . Similarly, write  $\mu_J(\mathbf{x}_*) = \hat{m}_* + \boldsymbol{\beta}^\top (\mathbf{y}_* - \hat{m}_* \mathbf{1}_{n_*})$  so that the the  $j^{\text{th}}$  component of  $\boldsymbol{\beta} = (\beta_1, \dots, \beta_{n_*})$  has the following form.

$$\beta_j = ((\sigma^2 \mathbf{I}_{n_*} + \mathbf{C}_{**})^{-1} \mathbf{c}_*)_j$$

Using  $\alpha_i$ 's and  $\beta_j$ 's set up as defined above, we may write (5) as

$$\begin{aligned} \mu_J(\mathbf{x}_*) &= \sum_{i \in \mathcal{D}_{n,*}} \alpha_i y_{i,*} + \sum_{j \in \mathcal{D}_{n,*}} \beta_j \left( y_{j,*} - \sum_{i \in \mathcal{D}_{n,*}} \alpha_i y_{i,*} \right) \\ &= \sum_{i \in \mathcal{D}_{n,*}} \alpha_i y_{i,*} + \sum_{j \in \mathcal{D}_{n,*}} \sum_{i \in \mathcal{D}_{n,*}} \alpha_i \beta_j (y_{j,*} - y_{i,*}), \end{aligned} \quad (18)$$

using that  $\sum_{i \in \mathcal{D}_{n,*}} \alpha_i = 1$ . The decomposition in Eq. (18) may be used estimate the bias of the mean predictor  $\mu_J(\mathbf{x}_*)$ :

$$\begin{aligned} \text{Bias}[\mu_J(\mathbf{x}_*)] &= \mathbb{E}[\mu_J(\mathbf{x}_*) - f(\mathbf{x}_*)] \\ &= \sum_{i \in \mathcal{D}_{n,*}} \alpha_i (\mathbb{E}[y_{i,*}] - \mathbb{E}[f(\mathbf{x}_*)]) + \sum_{i,j \in \mathcal{D}_{n,*}} \alpha_i \beta_j (\mathbb{E}[y_{j,*}] - \mathbb{E}[y_{i,*}]). \end{aligned} \quad (19)$$

Based on the assumption of the theorem, we can limit  $\mathbb{E}[y_{i,*}]$  (or  $\mathbb{E}[f(\mathbf{x}_*)]$ ) to only two possible values:  $m_*$  when  $\mathbf{x}_{i,*}$  (or  $\mathbf{x}_*$ ) is in  $\mathcal{D}_{n,*}$  and another value, say  $m_o$ , otherwise. Then, we can write

$$\begin{aligned} \mathbb{E}[y_{i,*}] - \mathbb{E}[f(\mathbf{x}_*)] &= (\mathbb{E}[y_{i,*}|Z_i = 1] - \mathbb{E}[f(\mathbf{x}_*)|Z_* = 0])p(Z_i = 1)p(Z_* = 0) \\ &\quad + (\mathbb{E}[y_{i,*}|Z_i = 0] - \mathbb{E}[f(\mathbf{x}_*)|Z_* = 1])p(Z_i = 0)p(Z_* = 1) \\ &= (m_* - m_o)\{p(Z_j = 0)p(Z_* = 1) - p(Z_i = 1)p(Z_* = 0)\}, \end{aligned}$$

where  $Z_*$  stands for the latent  $Z$ -variable associated with test point  $\mathbf{x}_*$ . Similarly,

$$\begin{aligned} \mathbb{E}[y_{j,*}] - \mathbb{E}[y_{i,*}] &= (\mathbb{E}[y_{j,*}|Z_j = 1] - \mathbb{E}[y_{i,*}|Z_i = 0])p(Z_j = 1)p(Z_i = 0) \\ &\quad + (\mathbb{E}[y_{j,*}|Z_j = 0] - \mathbb{E}[y_{i,*}|Z_i = 1])p(Z_j = 0)p(Z_i = 1) \\ &= (m_* - m_o)\{p(Z_i = 0)p(Z_j = 1) - p(Z_i = 1)p(Z_j = 0)\}. \end{aligned}$$

Let  $p_j$  and  $p_*$  represent  $P(Z_j = 1)$  and  $P(Z_* = 1)$ , respectively. Using the two quantities established above, the bias is

$$\begin{aligned} \text{Bias}[\mu_J(\mathbf{x}_*)] &= (m_* - m_o) \sum_{j \in \mathcal{D}_{n,*}} \alpha_j \{(1 - p_j)p_* - p_j(1 - p_*)\} \\ &\quad + (m_* - m_o) \sum_{i \in \mathcal{D}_{n,*}} \sum_{j \in \mathcal{D}_{n,*}} \alpha_j \beta_i \{p_j(1 - p_i) - (1 - p_j)p_i\}. \end{aligned} \quad (20)$$

## References

- Abrahamsen, P. (1997), ‘A review of Gaussian random fields and correlation functions’, Norsk Regnesentral/Norwegian Computing Center Oslo, [https://www.nr.no/directdownload/917\\_Rapport.pdf](https://www.nr.no/directdownload/917_Rapport.pdf).
- Beck, J. & Guillas, S. (2016), ‘Sequential design with mutual information for computer experiments (MICE): Emulation of a tsunami model’, *SIAM/ASA Journal on Uncertainty Quantification* **4**(1), 739–766.
- Binois, M., Gramacy, R. & Ludkovski, M. (2018), ‘Practical heteroscedastic Gaussian process modeling for large simulation experiments’, *Journal of Computational and Graphical Statistics* **27**(4), 808–821.  
**URL:** <https://doi.org/10.1080/10618600.2018.1458625>
- Binois, M., Huang, J., Gramacy, R. & Ludkovski, M. (2019), ‘Replication or exploration? Sequential design for stochastic simulation experiments’, *Technometrics* **27**(4), 808–821.  
**URL:** <https://doi.org/10.1080/00401706.2018.1469433>
- Bryant, P. & Williamson, J. A. (1978), ‘Asymptotic behaviour of classification maximum likelihood estimates’, *Biometrika* **65**(2), 273–281.
- Cohn, D. A., Ghahramani, Z. & Jordan, M. I. (1996), ‘Active learning with statistical models’, *Journal of Artificial Intelligence Research* **4**(1), 129–145.
- Damianou, A. & Lawrence, N. D. (2013), Deep Gaussian processes, in C. M. Carvalho & P. Ravikumar, eds, ‘Proceedings of the Sixteenth International Conference on Artificial Intelligence and Statistics’, Vol. 31 of *Proceedings of Machine Learning Research*, PMLR, Scottsdale, Arizona, USA, pp. 207–215.
- Dempster, A., Laird, N. & Rubin, D. (1977), ‘Maximum likelihood from incomplete data via the em algorithm’, *Journal of the Royal Statistical Society* **39**(1), 1–38.
- Gneiting, T. & Raftery, A. E. (2007), ‘Strictly proper scoring rules, prediction, and estimation’, *Journal of the American Statistical Association* **102**(477), 359–378.

- Gramacy, R. B. (2020), *Surrogates: Gaussian Process Modeling, Design, and Optimization for the Applied Sciences*, CRC Press, Boca Raton, FL, USA.
- Gramacy, R. B. & Apley, D. W. (2015), ‘Local Gaussian process approximation for large computer experiments’, *Journal of Computational and Graphical Statistics* **24**(2), 561–578.
- Gramacy, R. B. & Lee, H. K. (2009), ‘Adaptive design and analysis of supercomputer experiments’, *Technometrics* **51**(2), 130–145.
- Gramacy, R. B. & Lee, H. K. H. (2008), ‘Bayesian treed Gaussian process models with an application to computer modeling’, *Journal of the American Statistical Association* **103**(483), 1119–1130.
- Gramacy, R., Niemi, J. & Weiss, R. (2014), ‘Massively parallel approximate Gaussian process regression’, *SIAM/ASA Journal on Uncertainty Quantification* **2**(1), 564–584.
- Gramacy, R. & Taddy, M. (2016), **tgp**: *Bayesian Treed Gaussian Process Models*. R package version 2.4-14.  
**URL:** <https://CRAN.R-project.org/package=tgp>
- Gupta, M. R. & Chen, Y. (2010), ‘Theory and use of the EM algorithm’, *Foundations and Trends in Signal Processing* **4**(3), 223–296.
- Hastie, T., Tibshirani, R. & Friedman, J. (2009), *The elements of statistical learning: data mining, inference, and prediction*, Springer, New York, NY.
- Heaton, M. J., Christensen, W. F. & Terres, M. A. (2017), ‘Nonstationary Gaussian process models using spatial hierarchical clustering from finite differences’, *Technometrics* **59**(1), 93–101.
- Hwang, I. & Jang, Y. J. (2020), ‘Q ( $\lambda$ ) learning-based dynamic route guidance algorithm for overhead hoist transport systems in semiconductor fabs’, *International Journal of Production Research* **58**(4), 1199–1221.

- Kang, B., Park, C., Kim, H. & Hong, S. (2022), ‘Bayesian optimization for the vehicle dwelling policy in a semiconductor wafer fab’, *IEEE Transactions on Automation Science and Engineering* **submitted**, 1–21.
- Kim, H.-M., Mallick, B. K. & Holmes, C. C. (2005), ‘Analyzing nonstationary spatial data using piecewise Gaussian processes’, *Journal of the American Statistical Association* **100**(470), 653–668.
- Konomi, B. A., Sang, H. & Mallick, B. K. (2014), ‘Adaptive Bayesian nonstationary modeling for large spatial datasets using covariance approximations’, *Journal of Computational and Graphical Statistics* **23**(3), 802–829.
- Krause, A., Singh, A. & Guestrin, C. (2008), ‘Near-optimal sensor placements in Gaussian processes: Theory, efficient algorithms and empirical studies’, *Journal of Machine Learning Research* **9**(Feb), 235–284.
- Lam, C. Q. & Notz, W. (2008), ‘Sequential adaptive designs in computer experiments for response surface model fit’, *Statistics and Applications* **6**(1), 207–233.
- Lin, C. & Tang, B. (2015), ‘Latin hypercubes and space-filling designs’, *Handbook of Design and Analysis of Experiments* pp. 593–625.
- Luo, Z., Sang, H. & Mallick, B. (2021), ‘A Bayesian contiguous partitioning method for learning clustered latent variables’, *Journal of Machine Learning Research* **22**, 1–52.
- Magrez, A., Seo, J. W., Smajda, R., Mionić, M. & Forró, L. (2010), ‘Catalytic CVD synthesis of carbon nanotubes: towards high yield and low temperature growth’, *Materials* **3**(11), 4871–4891.
- Malloy, M. L. & Nowak, R. D. (2014), ‘Near-optimal adaptive compressed sensing’, *IEEE Transactions on Information Theory* **60**(7), 4001–4012.
- McKay, M. D., Beckman, R. J. & Conover, W. J. (2000), ‘A comparison of three methods for selecting values of input variables in the analysis of output from a computer code’, *Technometrics* **42**(1), 55–61.



- Mitchell, T. (1997), *Machine Learning*, McGraw-Hill, Inc, New York, NY.
- Mu, R., Dai, L. & Xu, J. (2017), ‘Sequential design for response surface model fit in computer experiments using derivative information’, *Communications in Statistics - Simulation and Computation* **46**(2), 1148–1155.
- Nikolaev, P., Hooper, D., Webber, F., Rao, R., Decker, K., Krein, M., Poleski, J., Barto, R. & Maruyama, B. (2016), ‘Autonomy in materials research: A case study in carbon nanotube growth’, *npj Computational Materials* **2**, 16031.
- Paciorek, C. & Schervish, M. (2006), ‘Spatial modelling using a new class of nonstationary covariance functions’, *Environmetrics* **17**(5), 483–506.
- Park, C. (2022), ‘Jump Gaussian process model for estimating piecewise continuous regression functions’, *Journal of Machine Learning Research* **23**(278), 1–37.
- Park, C., Qiu, P., Carpena-Núñez, J., Rao, R., Susner, M. & Maruyama, B. (2023), ‘Sequential adaptive design for jump regression estimation’, *IISE Transactions* **55**(2), 111–128.  
**URL:** <https://doi.org/10.1080/24725854.2021.1988770>
- Pope, C. A., Gosling, J. P., Barber, S., Johnson, J. S., Yamaguchi, T., Feingold, G. & Blackwell, P. G. (2021), ‘Gaussian process modeling of heterogeneity and discontinuities using Voronoi tessellations’, *Technometrics* **63**(1), 53–63.
- Rasmussen, C. & Williams, C. (2006), *Gaussian Processes for Machine Learning*, MIT Press, Cambridge, MA.
- Salimbeni, H. & Deisenroth, M. (2017), Doubly stochastic variational inference for deep Gaussian processes, *in* I. Guyon, U. V. Luxburg, S. Bengio, H. Wallach, R. Fergus, S. Vishwanathan & R. Garnett, eds, ‘Advances in Neural Information Processing Systems’, Vol. 30, Long Beach, CA, USA.
- Sampson, P. & Guttorp, P. (1992), ‘Nonparametric estimation of nonstationary spatial covariance structure’, *Journal of the American Statistical Association* **87**(417), 108–119.

- Santner, T. J., Williams, B. J., Notz, W. I. & Williams, B. J. (2003), *The design and analysis of computer experiments*, Springer, New York, NY.
- Santner, T., Williams, B. & Notz, W. (2018), *The Design and Analysis of Computer Experiments, Second Edition*, Springer–Verlag, New York, NY.
- Sauer, A., Gramacy, R. B. & Higdon, D. (2020), ‘Active learning for deep Gaussian process surrogates’, *arXiv preprint arXiv:2012.08015* .
- Schmidt, A. & O’Hagan, A. (2003), ‘Bayesian inference for non-stationary spatial covariance structure via spatial deformations’, *Journal of the Royal Statistical Society: Series B* **65**(3), 743–758.
- Siebert, M., Bartlett, K., Kim, H., Ahmed, S., Lee, J., Nazzal, D., Nemhauser, G. & Sokol, J. (2018), ‘Lot targeting and lot dispatching decision policies for semiconductor manufacturing: optimisation under uncertainty with simulation validation’, *International Journal of Production Research* **56**(1-2), 629–641.
- Taddy, M. A., Gramacy, R. B. & Polson, N. G. (2011), ‘Dynamic trees for learning and design’, *Journal of the American Statistical Association* **106**(493), 109–123.
- Wendland, H. (2004), *Scattered Data Approximation*, Cambridge University Press, Cambridge, England.
- Yang, T., Rajasekharan, M. & Peters, B. A. (1999), ‘Semiconductor fabrication facility design using a hybrid search methodology’, *Computers & Industrial Engineering* **36**(3), 565–583.